Mon. Not. R. Astron. Soc. **355,** 1010–1030 (2004) doi:10.1111/j.1365-2966.2004.08408.x

Cosmic evolution of quasar clustering: implications for the host haloes

Cristiano Porciani,[1]* Manuela Magliocchetti[2] and Peder Norberg[1]
[1] *Institute for Astronomy, ETH Hönggerberg, CH-8093 Zürich, Switzerland*
[2] *SISSA, Via Beirut 4, 34014, Trieste, Italy*

Accepted 2004 September 1. Received 2004 September 1; in original form 2004 June 1

ABSTRACT

We present detailed clustering measurements from the 2dF Quasi-Stellar Object Redshift Survey (2QZ) in the redshift range $0.8 < z < 2.1$. Using a flux-limited sample of ∼14 000 objects with effective redshift $z_{\rm eff} = 1.47$, we estimate the quasar projected correlation function for separations $1 < r/\,h^{-1}$ Mpc < 20. We find that the two-point correlation function in real space is well approximated by a power law with slope $\gamma = 1.5 \pm 0.2$ and comoving correlation length $r_0 = 4.8^{+0.9}_{-1.5}\,h^{-1}$ Mpc. Splitting the sample into three subsets based on redshift, we find evidence for an increase of the clustering amplitude with look-back time. For a fixed γ, evolution of r_0 is detected at the 3.6σ confidence level. The ratio between the quasar correlation function and the mass autocorrelation function (derived adopting the concordance cosmological model) is found to be scale-independent. For a linear mass-clustering amplitude $\sigma_8 = 0.8$, the 'bias parameter' decreases from $b \simeq 3.9$ at $z_{\rm eff} = 1.89$ to $b \simeq 1.8$ at $z_{\rm eff} = 1.06$. From the observed abundance and clustering, we infer how quasars populate dark matter haloes of different masses. We find that 2QZ quasars sit in haloes with $M > 10^{12}\,{\rm M}_\odot$ and that the characteristic mass of their host haloes is of the order of $10^{13}\,{\rm M}_\odot$. The observed clustering is consistent with assuming that the locally observed correlation between black hole mass and host galaxy circular velocity is still valid at $z > 1$. From the fraction of haloes which contain active quasars, we infer that the characteristic quasar lifetime is $t_{\rm Q} \sim$ a few $\times\,10^7$ yr at $z \sim 1$ and approaches 10^8 yr at higher redshifts.

Key words: galaxies: active – galaxies: clusters: general – quasars: general – cosmology: observations – cosmology: theory – large-scale structure of Universe.

1 INTRODUCTION

Recent dynamical studies have provided strong evidence for the existence of supermassive black holes in the centre of most nearby galaxies (for a review see, for example, Richstone et al. 1998). The mass of the central black hole seems to correlate with the luminosity and the velocity dispersion of the spheroidal stellar component (e.g. Magorrian et al. 1998; Ferrarese & Merritt 2000; Gebhardt et al. 2000; Tremaine et al. 2002). The surprising tightness of the latter relation suggests the existence of a strong connection between the formation of supermassive black holes and the assembly of galactic spheroids (Silk & Rees 1998; Haehnelt & Kauffmann 2000; Kauffmann & Haehnelt 2000; Monaco, Salucci & Danese 2000; Granato et al. 2004).

The mounting evidence for the presence of supermassive black holes in nearby galaxies supports the theoretical belief that quasars are powered by black hole accretion (Salpeter 1964; Zel'dovich & Novikov 1964; Lynden-Bell 1969). For instance, the locally estimated mass density in black holes and the observed evolution of the quasar luminosity function seem to be consistent with this hypothesis (Haehnelt, Natarajan & Rees 1998; Fabian & Iwasawa 1999; Salucci et al. 1999; Yu & Tremaine 2002; Wyithe & Loeb 2003; Marconi et al. 2004). However, a detailed understanding of the physical processes leading to quasar activity (and their connection with galaxy formation) is still lacking. For this reason, even simple phenomenological models that are able to reproduce the observational results by selecting which cosmic structures could harbour quasars are of paramount importance.

In the currently favoured cosmological model, galaxies are expected to form within extended dark matter haloes. At every epoch, the number density and clustering properties of the haloes can be readily (and reliably) computed as a function of their mass. It is therefore of great interest to try to establish a connection between these haloes and different classes of cosmic objects. Even though the distribution of light sources within haloes is determined by complex physics, some of its properties can be computed with a purely statistical approach. For instance, we can use the mean density and the clustering amplitude of a population of cosmic objects to determine the lowest-order moments of the 'halo occupation distribution

*E-mail: porciani@phys.ethz.ch

function', $P_N(M)$, which gives the probability of finding a given number of sources in a halo of mass M (e.g. Scoccimarro et al. 2001, and references therein). A number of 'halo models' have been presented in the literature. These have been successfully used to describe the abundance and clustering properties of galaxies at both low (Peacock & Smith 2000; Seljak 2000; Scoccimarro et al. 2001; Berlind & Weinberg 2002; Marinoni & Hudson 2002; Magliocchetti & Porciani 2003; van den Bosch, Mo & Yang 2003; Yang, Mo & van den Bosch 2003; Zehavi et al. 2004) and high (Bullock, Wechsler & Somerville 2002; Moustakas & Somerville 2002; Hamana et al. 2004; Zheng 2004) redshift. One of the main goals of this paper is to use a similar approach to investigate how quasars populate dark matter haloes. As previously discussed, this requires an accurate determination of the clustering properties of bright quasi-stellar objects (QSOs).

Since the first detection of quasar clustering (Shaver 1984; Shanks et al. 1987), a number of surveys (continuously improved in terms of homogeneity, completeness and size) have been used to measure the two-point correlation function of bright QSOs (Iovino & Shaver 1988; Andreani & Cristiani 1992; Mo & Fang 1993; Andreani et al. 1994; Shanks & Boyle 1994; Croom & Shanks 1996; La Franca, Andreani & Cristiani 1998; Grazian et al. 2004). The emerging picture is that quasars at $z \sim 1.5$ have a correlation length $r_0 \simeq 5 - 6\,h^{-1}$ Mpc, similar to that of present-day galaxies. It still is a matter of debate, however, whether r_0 significantly evolves with redshift (Iovino & Shaver 1988; Croom & Shanks 1996; La Franca et al. 1998). This uncertainty is due to the joint effects of cosmic variance and small-number statistics; given the sparseness of the quasar distribution, a typical sample includes from a few hundred to a thousand objects. In consequence, clustering is generally detected at a relatively low significance level (3–4σ).

The development of efficient multi-object spectrographs has recently made possible a new generation of wide-area redshift surveys. Both the completed 2dF QSO Redshift Survey (2QZ; Croom et al. 2004) and the ongoing Sloan Digital Sky Survey (SDSS) Quasar Survey (Schneider et al. 2003) list redshifts for tens of thousands of optically selected quasars. A preliminary data release of the 2QZ has been used to estimate the evolution and the luminosity dependence of the quasar two-point correlation function in redshift space (Croom et al. 2001, 2002). The final catalogue has been used to measure the quasar power spectrum out to scales of $500\,h^{-1}$ Mpc (Outram et al. 2003; see also Hoyle et al. 2002) and to constrain the cosmological constant from redshift-space distortions (Outram et al. 2004).

In this paper, we study the clustering properties of ~14 000 quasars extracted from the complete 2QZ. In particular, we compute the evolution of their projected two-point correlation function. This quantity is not affected by the distortion of the clustering pattern induced by peculiar motions as it measures the clustering strength as a function of quasar separation in the perpendicular direction to the line of sight. Using the largest quasar sample presently available, we are able to accurately measure the real-space clustering amplitude in three redshift bins. Our results reveal a statistically significant evolution of the clustering length with redshift.

We then combine our clustering study with the halo model to infer the mean number of optically selected quasars which are harboured by a virialized halo of given mass (the halo occupation number) and the characteristic quasar lifetime. Our results can be directly used to test physical models for black hole accretion.

The layout of the paper is as follows. In Section 2 we present our quasar samples, we measure their projected correlation function and we estimate the corresponding bias parameters. In Section 3, we introduce the halo model and we discuss how the halo occupation number, $N(M)$, is constrained by the observed abundance and clustering amplitude of optically bright quasars. Using the empirical correlation between black hole mass and circular velocity of the host galaxy (Ferrarese 2002), in Section 4 we present a new derivation of the function $N(M)$ based on the observed quasar luminosity function. We then show that this model is in agreement with the clustering measurements presented in Section 2. In Section 5, we present a Bayesian study of the halo occupation number which combines the results from Sections 3 and 4. This allows us to fully constrain all the parameters of the halo model. Estimates of the quasar lifetime are presented in Section 6 while the evolution of the halo occupation number over the redshift range $0.8 < z < 2.1$ is addressed in Section 7. Eventually, we discuss our results in Section 8 and conclude in Section 9.

Throughout this paper, we assume that the mass density parameter $\Omega_0 = 0.3$ (with a baryonic contribution $\Omega_b = 0.049$), the vacuum energy density parameter $\Omega_\Lambda = 0.7$ and the present-day value of the Hubble constant $H_0 = 100\,h$ km s^{-1} Mpc^{-1} with $h = 0.7$. We also adopt a cold dark matter (CDM) power spectrum with primordial spectral index $n = 1$ and $\sigma_8 = 0.8$ (with σ_8 being the rms linear density fluctuation within a sphere with a radius of $8\,h^{-1}$ Mpc). This is consistent with the most recent joint analyses of temperature anisotropies in the cosmic microwave background (CMB) and galaxy clustering (see, for example, Tegmark et al. 2004 and references therein) and with the observed quasar power spectrum (Outram et al. 2003).

2 THE DATA

In this section, we present the main properties of our data set and compute its clustering properties as a function of redshift.

2.1 Quasar selection and sample definitions

The 2QZ is a homogeneous data base containing the spectra of 44 576 stellar-like objects with $18.25 \leqslant b_J \leqslant 20.85$ (Croom et al. 2004). Selection of the quasar candidates is based on broad-band colours (ub_Jr) from automated plate measurements (APMs) of United Kingdom Schmidt Telescope (UKST) photographic plates. Spectroscopic observations with the 2dF instrument (a multifibre spectrograph) at the Anglo-Australian Telescope have been used to determine the intrinsic nature of the sources. The full survey includes 23 338 quasars (the vast majority of which are endowed with a high-quality identification and/or redshift) which span a wide redshift range ($0.3 \lesssim z \lesssim 2.9$) and are spread over 721.6 deg^2 on the sky (see Croom et al. 2004 for further details).

The 2QZ is affected by incompleteness in a number of different ways (for a detailed discussion, see Croom et al. 2004). In order to minimize systematic effects, we restrict our analysis to a subsample of sources defined by a minimum spectroscopic sector completeness of 70 per cent.[1] Moreover, we only consider regions of the 2QZ catalogue for which the photometric completeness is greater than 90 per cent; this corresponds to a redshift range $0.5 < z < 2.1$. Finally, we impose a cut in absolute magnitude, so that we only consider quasars brighter than $M_{b_J} - 5\log_{10} h = -21.7$, which, assuming $h = 0.7$, is equivalent to $M_{b_J} = -22.5$. Such an absolute magnitude

[1] A sector is a unique area on the sky defined by the intersection of a number of circular 2dF fields.

Table 1. Main properties of our data sets. The superscripts min, max and med denote the minimum, maximum and median values of a variable, respectively.

$z_{\rm min}$	$z_{\rm max}$	$z_{\rm eff}$	$M^{\rm min}$	$M^{\rm max}$ $M_{b_J} - 5\log_{10} h$	$M^{\rm med}$	$N_{\rm QSO}$	$n_{\rm QSO}$ 10^{-6} h^3 Mpc^{-3}	$b_J^{\rm med}$
0.8	1.3	1.06	−25.32	−21.72	−23.13	4928	8.54 ± 0.47 ± 0.85	19.95
1.3	1.7	1.51	−25.97	−22.80	−23.84	4737	7.20 ± 0.35 ± 0.72	20.02
1.7	2.1	1.89	−26.44	−23.37	−24.30	4324	6.21 ± 0.26 ± 0.62	20.07
0.8	2.1	1.47	−26.44	−21.72	−23.82	13 989	11.49 ± 1.52 ± 1.15	20.02

cut ensures the exclusion of quasars where the contribution from the host galaxy may have led to a mis-identification of the source.

In order to detect possible evolutionary effects, we want to subdivide our sample into three redshift bins. In particular, we require that (i) a similar number of quasars lie in each redshift bin, and (ii) each subsample covers a not too different interval of cosmic time. For this reason, we revise our initial sample selection by imposing an additional redshift cut, so as to keep only objects within $0.8 < z < 2.1$. In fact, the time interval covered by the redshift range $0.5 < z < 0.8$ (1.78 Gyr) corresponds to one-third of the total time elapsed between $z = 2.1$ and $z = 0.5$ (5.35 Gyr), whereas the number of quasars with $0.5 < z < 0.8$ represents less than 10 per cent of the selected quasar sample. By restricting the analysis to $0.8 < z < 2.1$, we can greatly improve on both the previously mentioned conditions. Moreover, we obtain a sample for which the mean number density of quasars is very weakly varying with redshift (as can be seen in fig. 1 of Outram et al. 2003), because through this cut we remove the largest mean number density variations as a function of redshift. The drop in mean density is less than 60 per cent between $z = 0.8$ and $z = 2.1$.

With the above selection, we end up with nearly 14 000 quasars [split in two regions, the North Galactic Pole (NGP) and South Galactic Pole (SGP) strips, with respectively ∼7800 and ∼6100 quasars each] of which 75 per cent reside in regions with total completeness larger than 80 per cent. In order to study the evolution of quasar clustering, we divide this sample into three redshift slices. To satisfy our previously mentioned criteria, we end up choosing the following three intervals, $0.8 < z < 1.3$, $1.3 < z < 1.7$ and $1.7 < z < 2.1$, each containing between ∼4300 and ∼4900 quasars (see Table 1). We note that the time covered between $z = 0.8$ and $z = 1.3$ (1.91 Gyr) is nearly twice the time covered between $z = 1.3$ and $z = 1.7$ (0.97 Gyr); this is however unavoidable if we want to keep similar numbers of quasars in each redshift interval. As the sample is magnitude-limited, each redshift interval will correspond to quasars of different intrinsic luminosities, a point we address further in Section 2.2.

2.2 Quasar number density

Croom et al. (2004) provide an analytical fit for the b_J quasar luminosity function, in the case of sources brighter than $M_{b_J} - 5\log_{10} h \geqslant -21.7$ and for $0.4 < z < 2.1$. They model the optical luminosity function as a double power law in luminosity which, as a function of magnitude (number of quasars per unit magnitude per unit volume), becomes

$$\Phi(M_{b_J}, z) = \frac{\Phi^*}{10^{0.4\,\beta_1(M_{b_J} - M^\star_{b_J})} + 10^{0.4\,\beta_2(M_{b_J} - M^\star_{b_J})}}. \quad (1)$$

Here, the evolution is encoded in the redshift dependence of the characteristic magnitude $M^\star_{b_J} \equiv M^\star_{b_J}(z) = M^\star_{b_J}(0) - 1.08\,k\,\tau(z)$ where $\tau(z)$ is the fractional look-back time (in units of the present age of the Universe) at redshift z and k is a constant. A table with the best-fitting values for the parameters β_1, β_2, $M^\star_{b_J}(0)$ and k is provided by Croom et al. (2004), together with their statistical uncertainties.

Equation (1) can be used to compute the selection function of the 2QZ between $z_{\rm min} < z < z_{\rm max}$

$$S(z, z_{\rm min}, z_{\rm max}) = \frac{\int_{M^{\rm b}_{b_J}(z)}^{M^{\rm f}_{b_J}(z)} \Phi(M_{b_J}, z)\,{\rm d}M_{b_J}}{\int_{M^{\rm min}_{b_J}}^{M^{\rm max}_{b_J}} \Phi(M_{b_J}, z)\,{\rm d}M_{b_J}}, \quad (2)$$

where $M^{\rm b}_{b_J}(z)$ and $M^{\rm f}_{b_J}(z)$ denote, respectively, the brightest and faintest absolute magnitudes that are detectable at redshift z. These are obtained by using the K-correction from the composite quasar spectrum by Brotherton et al. (2001), and by assuming fixed apparent magnitude limits: $b_J^{\rm faint} = 18.25$ and $b_J^{\rm bright} = 20.85$. The integration limits in the denominator of equation (2) are $M^{\rm min}_{b_J} = \min_{(z_{\rm min}, z_{\rm max})} M^{\rm b}_{b_J}(z)$ and $M^{\rm max}_{b_J} = \max_{(z_{\rm min}, z_{\rm max})} M^{\rm f}_{b_J}(z)$. The comoving volume effectively surveyed is then given by

$$V_{\rm eff}(z_{\rm min}, z_{\rm max}) = \Omega_{\rm s} \int_{z_{\rm min}}^{z_{\rm max}} S(z, z_{\rm min}, z_{\rm max}) \left|\frac{{\rm d}V}{{\rm d}z\,{\rm d}\Omega}\right| {\rm d}z, \quad (3)$$

where $\Omega_{\rm s}$ denotes the solid angle covered by the survey and $|\,{\rm d}V/{\rm d}z\ {\rm d}\Omega|$ is the Jacobian determinant of the transformation between comoving and redshift-space coordinates, which gives the comoving volume element per unit redshift and solid angle. We can then estimate the mean number density of quasars by writing

$$n_{\rm QSO}(z_{\rm min}, z_{\rm max}) = \sum_{i=1}^{N_{\rm QSO}} \frac{w_i}{V_{\rm eff}(z_{\rm min}, z_{\rm max})}, \quad (4)$$

where $N_{\rm QSO}$ and $\sum_i w_i$ are, respectively, the total number of observed quasars in the range $z_{\rm min} < z < z_{\rm max}$ and its completeness weighted counterpart. Results obtained by applying equation (4) are listed in Table 1, where we summarize the main properties of our samples. Two types of errors are quoted for $n_{\rm QSO}$. Those listed first are determined by independently varying the four parameters which define the optical quasar luminosity function (i.e. β_1, β_2, $M^\star_{b_J}(0)$ and k) within their 1σ uncertainties as reported by Croom et al. (2004).[2] On top of this error, we quote a ∼10 per cent uncertainty on $n_{\rm QSO}$ due to the large-scale distribution of quasars; as in Outram et al. (2003), we typically find a ∼10 per cent difference in the number counts between the SGP and NGP. As this difference appears to be nearly constant as a function of redshift, we quote

[2] If the errors for the four parameters are statistically independent, the quoted values for $\Delta\ n_{\rm QSO}$ approximately give 1σ uncertainties, whereas, if the parameters are correlated (which they most certainly are), the quoted errors for $n_{\rm QSO}$ correspond to a higher confidence interval.

for all subsamples the same typical uncertainty due to large-scale structure. We note that our determination of $n_{\rm QSO}$ is independent of the normalization constant $\Phi^{\star}$ appearing in equation (1).

From the luminosity function we also compute the effective redshift of the different samples as $z_{\rm eff} = \sum_{i=1}^{N_{\rm QSO}} w_i\, z_i / \sum_{i=1}^{N_{\rm QSO}} w_i$ (see Table 1).

2.3 Quasar projected correlation function

The simplest statistic that can be used to quantify clustering in the observed quasar distribution is the two-point correlation function in redshift space, $\xi^{\rm obs}(r_\perp, \pi)$. This measures the excess probability over random to find a quasar pair separated by π along the line of sight and by $r_\perp$ in the plane of the sky. These separations are generally derived from the redshift and the angular position of each source, so that the inferred π includes a contribution from peculiar velocities. In consequence, the reconstructed clustering pattern in comoving space turns out to be a distorted representation of the real one and $\xi^{\rm obs}(r_\perp, \pi)$ is found to be anisotropic. To avoid this effect, and to determine the quasar clustering amplitude in real space, we can then use the 'projected correlation function', which is obtained by integrating $\xi^{\rm obs}(r_\perp, \pi)$ in the π direction

$$\frac{\Xi^{\rm obs}(r_\perp)}{r_\perp} = \frac{2}{r_\perp}\int_0^\infty \xi^{\rm obs}(r_\perp, \pi)\,{\rm d}\pi, \qquad (5)$$

and it is therefore unaffected by redshift-space distortions. In this section, we measure this quantity for our quasar samples.

We start by building a catalogue of unclustered points which has the same angular and radial selection function as the data. The angular selection is trivially given by the different completeness masks (see Croom et al. 2004 for further details), and we modulate the number of random points laid down as a function of spectroscopic and photometric completeness. The radial selection function is instead obtained by heavily smoothing the observed quasar redshift distribution, $\mathcal{N}(z)$, or even the observed quasar comoving distance distribution, $\mathcal{N}(r)$. Both uniform and Gaussian smoothings, with characteristic smoothing length of several hundreds of h^{-1} Mpc, have been used. The quoted results are insensitive to the precise details of the modelling of the radial selection function. This is partially due to the fact that the volume covered by the quasar sample is very large and that there are not many clear groups or clusters of quasars; the quasar redshift distribution is rather smooth when compared to a standard galaxy distribution (e.g. fig. 1 of Outram et al. 2003 versus fig. 13 of Norberg et al. 2002).

The quasar correlation function is then estimated by comparing the probability distribution of quasar and random pairs on a two-dimensional grid of separations $(r_\perp, \pi)$. We use both the Landy–Szalay estimator (Landy & Szalay 1993) and the Hamilton estimator (Hamilton 1993)

$$\xi^{\rm obs}_{\rm LS} = \frac{DD - 2DR + RR}{RR}, \quad \xi^{\rm obs}_{\rm H} = \frac{DD\,RR}{(DR)^2} - 1, \qquad (6)$$

where *DD*, *DR* and *RR* are the suitably normalized numbers of weighted data–data, data–random and random–random pairs in each bin.[3] As expected, the two estimators give comparable answers within the errors. For this reason, in what follows we only present results obtained with the Hamilton estimator.

[3] Note that, in this case, there is no need to use the standard J_3 (minimum variance) weighting scheme (Efstathiou 1988) because the mean density of quasars, $n_{\rm QSO}$, is so low that $1 + 4\pi\, J_3\, n_{\rm QSO} \simeq 1$ for any reasonable quasar clustering amplitude.

With the current quasar sample, we find that a reliable measure of $\xi^{\rm obs}(r_\perp, \pi)$ is only achievable on scales $\pi \lesssim 50\,h^{-1}$ Mpc. In fact, the number of quasar pairs with small transverse separations and large line-of-sight separation is very small. This is partially due to the sparseness of the samples considered but also to the rareness of large structures of quasars. Eventually, we compute the projected correlation function using equation (5). In order to avoid the measured signal being dominated by noise, we limit the integration to an upper limit, $\pi_{\rm max}$. This limiting value needs to be sufficiently large in order to give a reliable and meaningful measurement of $\Xi^{\rm obs}(r_\perp)/r_\perp$ on the scales of interest (i.e. $r_\perp \lesssim 20\,h^{-1}$ Mpc) but also small enough to be less sensitive to noise. Using the redshift distortion models by Hoyle et al. (2002), we find that $\pi_{\rm max} = 45\,h^{-1}$ Mpc fulfils both requirements. All the data presented in this paper are obtained using this value. In any case, we verify that our results are not sensitive to the precise value adopted for $\pi_{\rm max}$.

2.4 Error estimates for clustering measurements

It is common practice to estimate errors on the clustering measurements from mock surveys based on galaxy formation models. However, for quasars, such catalogues are not publicly available. We therefore opt for a bootstrap resampling technique. For each redshift interval, we divide both the NGP and SGP samples into eight equal-volume regions, and we measure the clustering properties of each subsample. For ease of calculation, the division is only based on redshift and is such that the depth of each region is larger than the adopted value for $\pi_{\rm max}$. Because the number density is roughly constant as a function of redshift, each of these regions approximately contains the same number of quasars. We then build 1000 bootstrap samples, each of them composed by 16 subsamples (eight for each strip) randomly drawn (allowing repetitions) from the set described above. We measure the projected correlation function for each artificial sample by appropriately averaging over the number of quasar and random pairs of the subsamples (and not over individual quasar clustering measurements). For each $r_\perp$, we identify the rms variation of Ξ over the bootstrap samples with the 1σ error for the projected correlation function.

Our method for estimating errors relies on the fact that our data set is statistically representative of the quasar distribution in the Universe. However, this cannot be true for bins of spatial separations which contain just a few quasar pairs. Therefore, in what follows, we ignore clustering results obtained by less than 20 quasar pairs. Depending on the sample, this corresponds to $r_\perp < 1$–$2\,h^{-1}$ Mpc. Note that, on such scales, corrections for close pair incompleteness due to fibre collisions (Croom et al. 2004) should also be taken into account.

2.5 Results

The projected correlation function we obtained for the different redshift bins (and for the total sample) is presented in the left-hand panel of Fig. 1. A clear evolutionary trend emerges from the data: the clustering amplitude for the high-redshift sample is nearly a factor of 2 (3) higher than for the total (low-redshift) sample.

As a zeroth-order approximation, we fit our results with a power-law functional form. This phenomenological description has been commonly used in the literature and allows us to compare our results with previous studies. More detailed modelling is presented in the next sections. Here, we assume that the quasar two-point correlation

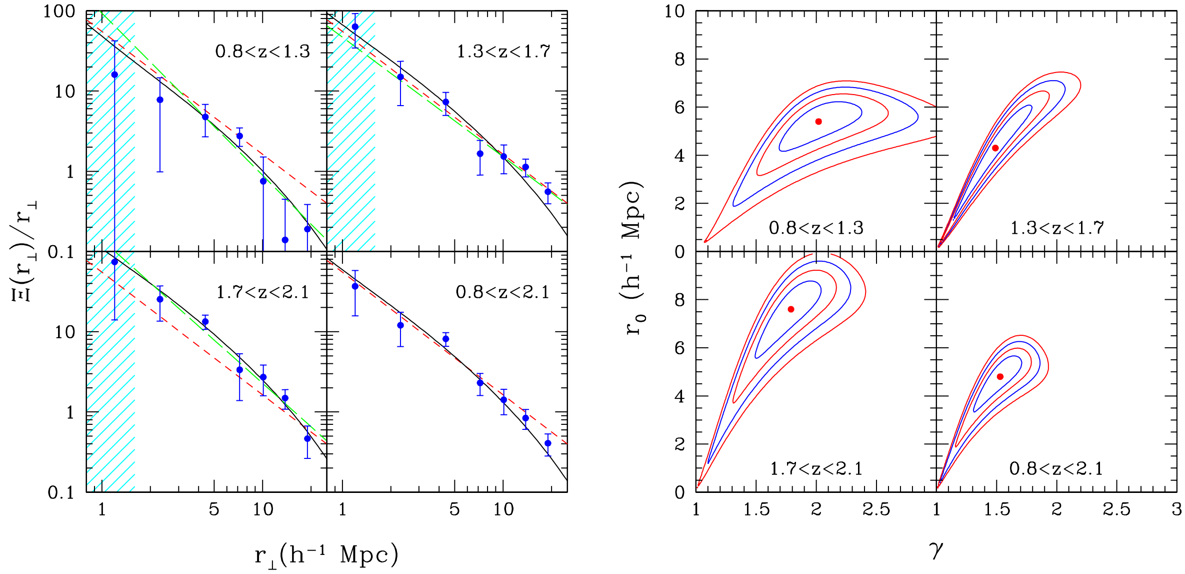

Figure 1. Left-hand panel: the projected correlation function for different samples of quasars from the 2QZ (data with error bars). For each redshift subsample, the best-fitting power law is represented with a long-dashed line. For reference, the best-fitting power law for the full sample ($0.8 < z < 2.1$) is shown with a short-dashed line. The solid lines represent the best-fitting constant bias models discussed in Section 2.7. These functions practically coincide with the best-fitting halo occupation models presented in Sections 3.4 and 5. Data in the shaded regions are derived from less than 20 quasar pairs and are not considered for model fitting. Right-hand panel: contour levels for the likelihood function obtained by fitting the data with a power-law model. The best-fitting models are marked with a dot and the lines correspond to four different values of $\Delta\chi^2 = \chi^2 - \chi^2_{\rm min}$. In particular, for Gaussian errors, the inner contours ($\Delta\chi^2 = 1$ and 2.3) mark the 68.3 per cent confidence levels for one and two parameters, respectively. Similarly, the outer contours ($\Delta\chi^2 = 4$ and 6.17) correspond to the 95.4 per cent confidence levels for one and two parameters.

function scales as

$$\xi(r) = \left(\frac{r_0}{r}\right)^{\gamma}, \quad (7)$$

where r denotes the comoving separation between quasar pairs. The corresponding projected correlation function is obtained through the simple integral relation,

$$\Xi(r_\perp) = 2\int_{r_\perp}^{\infty} \frac{r\,\xi(r)}{(r^2 - r_\perp^2)^{1/2}}\,\mathrm{d}r, \quad (8)$$

which, in the power-law case, reduces to

$$\frac{\Xi(r_\perp)}{r_\perp} = \frac{\Gamma(1/2)\,\Gamma[(\gamma-1)/2]}{\Gamma(\gamma/2)}\left(\frac{r_0}{r_\perp}\right)^{\gamma} \quad (9)$$

where $\Gamma(x)$ is the Euler Gamma function. We use a minimum least-squares method (corresponding to a maximum likelihood method in the case of Gaussian errors) to determine the values of r_0 and γ that best describe the clustering data. A principal component analysis (see, for example, Porciani & Giavalisco 2002) is used here to deal with correlated error bars. The principal components of the errors have been computed by diagonalizing the covariance matrix obtained by resampling the data with the bootstrap method described in the previous section. The objective function (the usual χ^2 statistic) has been obtained by considering the first four principal components which, for each redshift interval, account for more than 85 per cent of the variance.

The best-fitting values for γ and r_0 are given in Table 2 and the corresponding projected correlation functions are overplotted on the data in the left-hand panel of Fig. 1. Contour plots of the χ^2 functions are shown in the right-hand panel of Fig. 1. Note that the correlation length, r_0, and the slope of the correlation function, γ, are strongly covariant; in order to accurately describe the data, larger values of r_0 need to be associated with steeper slopes. The best-fitting slope for the whole quasar sample, $\gamma = 1.53^{+0.19}_{-0.21}$, is in very good agreement with the redshift-space analysis by Croom et al. (2001), who found $\gamma = 1.56^{+0.10}_{-0.09}$ at a mean redshift of $\bar{z} = 1.49$. This is not surprising, because we only consider scales that are in the quasi-linear and linear regimes of gravitational instability where the correlation functions in real and redshift space are proportional to each other (Kaiser 1987). Accordingly, the comoving correlation length we find in real space, $r_0 = 4.8^{+0.9}_{-1.5}\,h^{-1}$ Mpc, is, as expected, slightly smaller than its redshift-space counterpart, $5.69^{+0.42}_{-0.50}\,h^{-1}$ Mpc.[4]

As previously discussed, visual inspection of Fig. 1 suggests that the quasar clustering amplitude at $1.7 < z < 2.1$ is nearly a factor of 2 higher than that obtained for the whole sample. 2σ evidence for an increase in the clustering amplitude of optically selected quasars between $z \sim 1$ and $z \sim 1.8$ has been presented by La Franca et al. (1998). However, given their sample size (a few hundred quasars) it is not clear whether the detected evolution is real or whether it is spuriously created by cosmic variance effects; see, for example, the discussion in Croom et al. (2001) who, using a preliminary data release of the 2QZ, found that the redshift-space clustering amplitude at $z = 2.7$ is a factor of 1.4 higher than at $z = 0.7$, which is marginally significant. It is therefore interesting to try to quantify the evolution of the clustering amplitude in our large quasar sample. In order to facilitate the comparison among the different subsamples (and with previous studies), we report in Table 2 the 68.3 per cent confidence intervals for r_0 obtained by assuming $\gamma = 1.53$ [$r_0^{(\gamma=1.53)}$] and $\gamma = 1.80$ [$r_0^{(\gamma=1.80)}$]. When fixing the slope, we note a steady increase of the quasar correlation length with z. Within this approximation, clustering evolution with redshift is detected at

[4] Croom et al. (2001) assume statistically independent Poisson error bars for the correlation function at different separations. This explains the factor of 2 between their estimate and our estimate of the uncertainty for r_0 and γ.

Table 2. Best-fitting power law and constant bias models for the four quasar samples. The goodness of each fit is measured by the quantity $\chi^2_{\rm min}/$ dof which gives the minimum value assumed by the χ^2 statistic divided by the number of degrees of freedom. M_b denotes the halo mass which matches the observed clustering amplitude.

$z_{\rm min}$	$z_{\rm max}$	r_0 (h^{-1} Mpc)	γ	$\frac{\chi^2_{\rm min}}{\rm dof}$	$r_0^{(\gamma=1.53)}$ (h^{-1} Mpc)	$\frac{\chi^2_{\rm min}}{\rm dof}$	$r_0^{(\gamma=1.8)}$ (h^{-1} Mpc)	$\frac{\chi^2_{\rm min}}{\rm dof}$	b	$\frac{\chi^2_{\rm min}}{\rm dof}$	$\log_{10}\frac{M_b}{\rm M_\odot}$
0.8	1.3	$5.4^{+0.9}_{-1.3}$	$2.02^{+0.36}_{-0.33}$	2.36/2	$3.4^{+0.6}_{-0.7}$	4.52/3	$4.7^{+0.7}_{-0.7}$	2.85/3	$1.80^{+0.20}_{-0.24}$	1.96/3	$12.80^{+0.20}_{-0.33}$
1.3	1.7	$4.3^{+1.8}_{-2.0}$	$1.49^{+0.32}_{-0.35}$	1.25/2	$4.6^{+0.4}_{-0.5}$	1.27/3	$6.0^{+0.4}_{-0.5}$	2.20/3	$2.62^{+0.18}_{-0.19}$	3.18/3	$13.00^{+0.11}_{-0.12}$
1.7	2.1	$7.6^{+1.2}_{-2.1}$	$1.79^{+0.25}_{-0.29}$	2.04/2	$5.9^{+0.7}_{-0.7}$	2.85/3	$7.6^{+0.8}_{-0.8}$	2.04/3	$3.86^{+0.32}_{-0.35}$	0.84/3	$13.26^{+0.11}_{-0.14}$
0.8	2.1	$4.8^{+0.9}_{-1.5}$	$1.53^{+0.19}_{-0.21}$	0.13/2	$4.8^{+0.6}_{-0.6}$	0.13/3	$5.4^{+0.5}_{-0.5}$	2.54/3	$2.42^{+0.20}_{-0.21}$	0.57/3	$12.91^{+0.13}_{-0.16}$

the $\sim$3.6σ confidence level. However, because we are dealing with a flux-limited sample (where the highest-redshift objects have, on average, the highest intrinsic luminosities), it is not possible to say whether this evolution of r_0 corresponds to a real change in the quasar population or to clustering segregation with luminosity. By analysing quasar clustering in the range $0.3 < z < 2.9$ as a function of apparent luminosity in the preliminary data release catalogue of the 2QZ, Croom et al. (2002) found weak ($\simeq 1\sigma$) evidence for the brightest third of quasars in the sky to be more clustered than the full data set. Even though the different selection criteria prevent a direct comparison, we find a statistically more significant change in the clustering strength among our subsamples than that reported in Croom et al. (2002). We defer a detailed analysis of the luminosity dependence of quasar clustering to future work.

2.6 Quasar versus galaxy clustering

How do our results on the spatial distribution of quasars compare with galaxy clustering at similar redshifts? Until very recently, only rather small samples of high-redshift galaxies were available and any attempt to determine their clustering properties was most probably hampered by cosmic variance (e.g. Le Fèvre et al. 1996; Carlberg et al. 1997; Arnouts et al. 1999; Magliocchetti & Maddox 1999). The advent of colour-selected surveys has allowed the detection of rich and homogeneous samples of high-redshift galaxies over relatively large volumes. We want to compare the results obtained from the largest samples presently available with those obtained from our sample of quasars. A number of studies have shown that Lyman-break galaxies at $z \sim 3$ are strongly clustered (e.g. Porciani & Giavalisco 2002 and references therein). Both their correlation length, $r_0 \sim 4\,h^{-1}$ Mpc, and the slope of ξ, $\gamma \sim 1.5$ (Porciani & Giavalisco 2002; Adelberger et al. 2003), are remarkably similar to the values obtained from our quasar sample. On the other hand, star-forming galaxies at $z \simeq 1$ (detected by exploiting the Balmer break in their spectra) are found to be slightly less clustered: $r_0 \sim 3\,h^{-1}$ Mpc with $\gamma \sim 1.7$ (Adelberger 2000). Similarly, the galaxy–galaxy correlation function from the DEEP2 Galaxy Redshift Survey at $z_{\rm eff} = 1.14$ is well described by a power law with $\gamma = 1.66 \pm 0.12$ and $r_0 = 3.1 \pm 0.7\,h^{-1}$ Mpc (Coil et al. 2004). Evidence that early-type galaxies are more clustered than late-type galaxies (Firth et al. 2002; Coil et al. 2004) might help us to reconcile these results with those inferred from the quasar population. Extremely red galaxies at $z \sim 1$ have been found to be exceptionally strongly clustered. Assuming $\gamma = 1.8$ (as inferred from their angular clustering) implies $r_0 \sim 12\,h^{-1}$ Mpc (Daddi et al. 2001; Firth et al. 2002; Roche, Dunlop & Almaini 2003).

2.7 Quasar versus dark matter clustering

To study how the spatial distribution of quasars relates to the underlying matter distribution, we introduce the quasar-to-mass bias function

$$b(r_\perp, z_{\rm eff}) = \left[\frac{\Xi(r_\perp, z_{\rm min} < z < z_{\rm max})}{\Xi_{\rm m}(r_\perp, z_{\rm eff})}\right]^{1/2} \qquad (10)$$

where $\Xi_{\rm m}$ is the projected correlation function of the mass distribution in the assumed cosmology computed as in Peacock & Dodds (1996). Fig. 2 shows our results for the different redshift bins. Error bars at different spatial separations are not statistically independent. As previously described, we fit the data with a constant function by using the principal components of the bootstrap errors (which shows that data points at $r_\perp > 10\,h^{-1}$ Mpc are strongly correlated). The results and the corresponding 1σ uncertainties are listed in Table 2. We find that b steadily increases with z. This statistically significant trend is mostly due to the rapid evolution of the mass autocorrelation function.

It is interesting to determine the halo mass, M_b, which corresponds to the observed quasar clustering amplitude (i.e. as if all quasars would reside in haloes with a fixed mass). We find that, for all the subsamples, M_b is of the order of 10^{13} $\rm M_\odot$ and that it slightly increases with z (see Table 2).

3 HALO OCCUPATION NUMBER OF QUASARS

In this section, we present the halo model for the spatial distribution of quasars. After introducing the basic notation, we describe the main features which characterize our model.[5] We then use the number density and the projected correlation function determined in Section 2 to constrain the free parameters of the halo model. This allows us to determine the way quasars populate dark matter haloes of different masses.

[5] Further details can be found in Magliocchetti & Porciani (2003) where we used a similar tool to study the clustering properties of galaxies with different spectral types in the 2dF Galaxy Redshift Survey (2dFGRS).

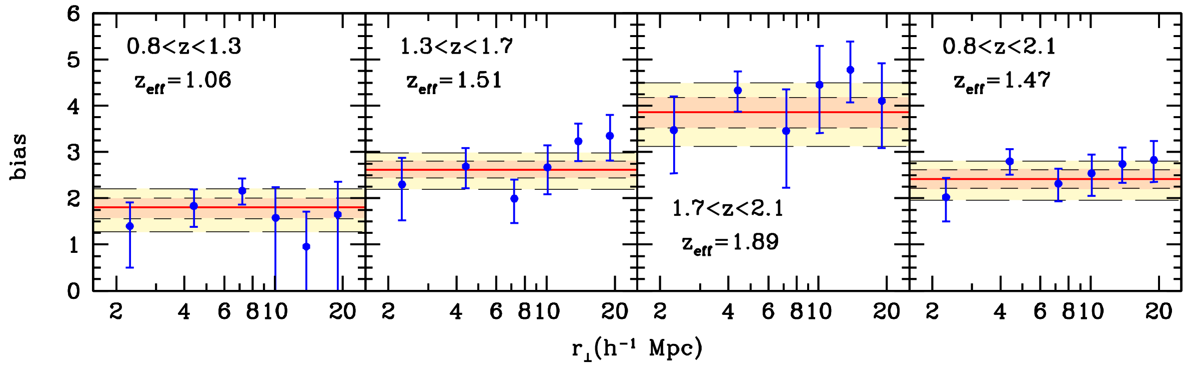

Figure 2. Quasar-to-mass bias function derived by applying equation (10) to quasar samples within different redshift ranges (points with error bars). The solid line shows the best-fitting constant value. Dashed lines indicate the values of the bias for which $\Delta\chi^2 = 1$ (short-dashed lines) and $\Delta\chi^2 = 4$ (long-dashed lines).

3.1 Halo model

It is generally believed that quasars are powered by mass accretion on to supermassive black holes lying at the centre of galaxies. CDM models for structure formation predict that galaxies form within extended dark matter haloes. The number density and clustering properties of these haloes can be easily computed, at any redshift, by means of a set of analytical tools which have been tested and calibrated against numerical simulations (e.g. Mo & White 1996; Sheth & Tormen 1999). In consequence, the problem of discussing the abundance and spatial distribution of quasars can be reduced to studying how they populate their host haloes. The basic quantity here is the halo occupation distribution function, $P_N(M)$, which gives the probability of finding N quasars within a single halo as a function of the halo mass, M. Given the halo mass function $n(M)$ (the number of dark matter haloes per unit mass and volume), the mean value of the halo occupation distribution $N(M) = \langle N\rangle(M) = \sum_N N\,P_N(M)$ (which from now on will be referred to as the halo occupation number) completely determines the mean comoving number density of quasars:

$$\bar{n} = \int n(M)\,N(M)\,\mathrm{d}M. \qquad (11)$$

Analogous relations, involving higher-order moments of $P_N(M)$, can be used to derive the clustering properties of quasars in the halo model. For instance, the two-point correlation function can be written as the sum of two terms

$$\xi(r) = \xi^{1\mathrm{h}}(r) + \xi^{2\mathrm{h}}(r). \qquad (12)$$

The function $\xi^{1\mathrm{h}}$, which accounts for pairs of quasars residing within the same halo, depends on the second factorial moment of the halo occupation distribution, $\Sigma^2(M) = \langle N(N-1)\rangle(M)$ and on the spatial distribution of quasars within their host haloes, $\rho(\boldsymbol{x}; M)$,[6]

$$\xi^{1\mathrm{h}}(r) = \int \frac{n(M)\,\Sigma^2(M)}{\bar{n}^2}\mathrm{d}M \int \rho(\boldsymbol{x}; M)\rho(\boldsymbol{x}+\boldsymbol{r}; M)\,\mathrm{d}^3x. \qquad (13)$$

On the other hand, the contribution to the correlation coming from quasars in different haloes, $\xi^{2\mathrm{h}}_{\mathrm{QSO}}$, depends on $N(M)$ and $\rho(\boldsymbol{x};M)$ as follows

$$\xi^{2\mathrm{h}}(r) = \int \frac{n(M_1)\,N(M_1)}{\bar{n}}\mathrm{d}M_1 \int \frac{n(M_2)\,N(M_2)}{\bar{n}}\,\mathrm{d}M_2 \times \int \rho(\boldsymbol{x}_1; M_1)\rho(\boldsymbol{x}_2; M_2) \times \xi_{\mathrm{h}}(\boldsymbol{r}_{12}; M_1, M_2)\,\mathrm{d}^3r_1\,\mathrm{d}^3r_2, \qquad (14)$$

where $\boldsymbol{r}_i$ marks the position of the centre of each halo, $\boldsymbol{r}_{12} = \boldsymbol{r}_2 - \boldsymbol{r}_1$ is the separation between the haloes, $\boldsymbol{x}_i$ denotes the quasar position with respect to each halo centre (hence $\boldsymbol{r} = \boldsymbol{r}_{12} + \boldsymbol{x}_2 - \boldsymbol{x}_1$), and $\xi_{\mathrm{h}}(r_{12}; M_1, M_2)$ is the cross-correlation function of haloes of mass M_1 and M_2, separated by r_{12}. For separations which are larger than the virial radius of the typical quasar-host halo, the two-halo term dominates the correlation function. In this regime, $\xi_{\mathrm{h}}(r; M_1, M_2)$ scales proportionally to the mass autocorrelation function, $\xi_{\mathrm{m}}(r)$, as $\xi_{\mathrm{h}}(r; M_1, M_2) \simeq b(M_1)\,b(M_2)\,\xi_{\mathrm{m}}(r)$, with $b(M)$ the linear-bias factor of haloes of mass M (Cole & Kaiser 1989; Mo & White 1996; Catelan et al. 1997; Porciani et al. 1998). As a consequence of this, the large-scale behaviour of the quasar correlation function also comes out to be $\xi(r) \simeq b^2_{\mathrm{eff}}\,\xi_{\mathrm{m}}(r)$, with

$$b_{\mathrm{eff}} = \frac{\int b(M)\,N(M)\,n(M)\,\mathrm{d}M}{\int N(M)\,n(M)\,\mathrm{d}M}. \qquad (15)$$

Note that all the different quantities introduced in this section depend on the redshift z, even though we have not made it explicit in the equations.

In order to use the halo model to study quasar clustering, we have to specify a number of functions describing the statistical properties of the population of dark matter haloes. In general, these have either been obtained analytically and then calibrated against N-body simulations, or directly extracted from numerical experiments. For the mass function and the linear bias factor of dark matter haloes, we adopt here the model by Sheth & Tormen (1999). We approximate the two-point correlation function of dark matter haloes with the function (see, for example, Porciani & Giavalisco 2002; Magliocchetti & Porciani 2003)

$$\xi_{\mathrm{h}}(r; M_1, M_2) = \begin{cases} b(M_1)\,b(M_2)\,\xi_{\mathrm{m}}(r) & \text{if } r \geqslant r_1 + r_2 \\ -1 & \text{if } r < r_1 + r_2 \end{cases}. \qquad (16)$$

Here, the mass autocorrelation function, $\xi_{\mathrm{m}}(r)$, is computed using the method introduced by Peacock & Dodds (1996), which, for our purposes, is sufficiently accurate both in the linear and

[6] This is normalized in such a way that $\int_0^{r_{\mathrm{vir}}} \rho(\boldsymbol{y}; M)\,\mathrm{d}^3y = 1$ where r_{vir} is the virial radius which is assumed to mark the outer boundary of the halo.

non-linear regimes.[7] For small separations, equation (16) accounts for spatial exclusion between haloes (e.g. two haloes cannot occupy the same volume). In Section 3.6, where we discuss the small-scale clustering of quasars, we identify the Eulerian zone of exclusion of a given halo, r_i, with its virial radius. At the same time, we assume that quasars trace the dark matter distribution and adopt, for $\rho(\boldsymbol{x}; M)$ a Navarro, Frenk & White (1997, hereafter NFW) profile with concentration parameter obtained from equations (9) and (13) of Bullock et al. (2001). Note that, in all the other sections of this paper, we only consider the large-scale distribution of quasars ($r \gtrsim 2\,h^{-1}$ Mpc), where exclusion effects and density profiles do not affect the predictions of the halo model for ξ.

3.2 Clustering on the light cone

Equations (12), (13) and (14) describe the clustering properties of a population of cosmic objects selected in a three-dimensional spatial section taken at constant cosmic time in the synchronous gauge. However, deep surveys such as the 2QZ span a wide interval of look-back times and the equations we have introduced above do not apply in this case.

A number of authors have discussed two-point statistics of objects lying on the light cone of the observer (e.g. Matarrese et al. 1997; Yamamoto & Suto 1999; Moscardini et al. 2000 and references therein). These works have shown that the observed correlation function can be written as the weighted average

$$\xi^{\rm obs}(r) = \frac{\int_{z_{\rm min}}^{z_{\rm max}} \mathcal{W}(z)\,\xi(r,z)\,{\rm d}z}{\int_{z_{\rm min}}^{z_{\rm max}} \mathcal{W}(z)\,{\rm d}z}. \tag{17}$$

Here $\mathcal{W}(z) = \mathcal{N}(z)^2({\rm d}V/{\rm d}z)^{-1}$, where $\mathcal{N}(z)$ is the actual redshift distribution of the objects in the sample and ${\rm d}V/{\rm d}z$ is the Jacobian between comoving volume and redshift. Note that equation (17) only holds for scales r over which (i) $\mathcal{N}$ is nearly constant and (ii) ξ does not significantly evolve over the time $r/[(1+z)c]$ (where c denotes the speed of light in vacuum). Within the range of separations covered by our data set, both the conditions are satisfied for our quasar sample.

Combining equations (8), (12) and (17), we compute $\Xi^{\rm obs}(r_\perp)$ in our four redshift intervals for a large set of $N(M)$ models and we then compare the results with $\Xi(r_\perp, z_{\rm eff})$, the constant-time correlation function evaluated by using equations (8) and (12) at the effective redshift of each subsample. In all cases we find extremely good agreement between the two functions. Even for the widest redshift bin, $0.8 < z < 2.1$, we find a maximum discrepancy of 2 per cent, which is negligibly small with respect to the typical error associated with the observed correlation function. Therefore, in what follows, we use $\Xi(r_\perp, z_{\rm eff})$ to compare the predictions of different models with the clustering data. This greatly simplifies (and speeds up) the model fitting procedure. As an additional test, the comparison between $\Xi^{\rm obs}(r_\perp)$ and $\Xi(r_\perp, z_{\rm eff})$ is repeated for all the best-fitting models that are discussed in the forthcoming sections, and no significant difference is found.

[7] In principle, for separations where $\xi_{\rm m}(r) \sim 1$, non-linear terms should be added to equation (16) (Mo & White 1996; Catelan et al. 1997; Porciani et al. 1998). However, for the haloes and redshifts of interest, these can be safely neglected.

3.3 Halo occupation number

The final, key ingredient needed to describe the clustering properties of quasars is their halo occupation distribution function. In the most general case, $P_N(M)$ is entirely specified by all its moments which, in principle, could be observationally determined by studying quasar clustering at any order. Regrettably, as we have already shown in Section 2.5, quasars are so rare that their two-point function is already very poorly determined, so that it is not possible to accurately measure higher-order statistics. As in Magliocchetti & Porciani (2003), we overcome this problem by assuming a predefined functional form for the lowest-order moments of $P_N(M)$. It is, in fact, convenient to describe the halo occupation number, $N(M)$, and (if necessary) its associated scatter, $\Sigma^2(M)$, in terms of a few parameters whose values will then be constrained by the data.

We consider here the 'censored' power-law model

$$N(M) = N_0 \left(\frac{M}{M_0}\right)^{\alpha} \Theta(M - M_0) \tag{18}$$

(where $\Theta(x)$ denotes the Heaviside probability distribution function) which has been widely used in the literature to describe galaxy clustering (e.g. Magliocchetti & Porciani 2003 and references therein). In this case, the halo occupation number vanishes for $M < M_0$ and scales as a power law of the halo mass for $M > M_0$. The parameter N_0 gives the mean number of objects contained in a halo of mass M_0.[8] Studies of the local galaxy population with both hydrodynamical simulations and semi-analytical models for galaxy formation are consistent with equation (18) (e.g. Sheth & Diaferio 2001; Berlind & Weinberg 2002; Berlind et al. 2003). We assume that the same parametrization is adequate for quasars at $z \gtrsim 1$. Given the observational evidence for a correlation between black hole and host halo masses (Ferrarese 2002; see also the discussion in Appendix A5), it is reasonable to expect the presence of a threshold mass for the host haloes of a quasar population with a given minimum luminosity. At the same time, a power-law scaling with an unspecified index α for $M > M_0$ is general enough to explore a wide range of possibilities.

It would be ideal to test equation (18) against physical models for quasar activity. A number of authors have recently developed simplified schemes to include black hole accretion in galaxy formation models (e.g. Kauffmann & Haehnelt 2002; Enoki, Nagashima & Gouda 2003; Menci et al. 2003; Di Matteo et al. 2003 and references therein). Regrettably, at variance with studies of normal galaxies, mock catalogues produced with these models are not publicly available. For this reason, to test the reliability of equation (18), we are forced to follow an indirect approach by associating quasar activity with a particular subset of synthetic galaxies. In particular, we consider galaxies which, at $z \gtrsim 1$, contain a substantial amount of cold gas in their nuclear region that, in principle, could be accreted on to a central supermassive black hole. Thus, in Appendix B, we use a publicly available semi-analytical model for galaxy formation (Hatton et al. 2003) to study the halo occupation number of galaxies which, at $z \sim 1$, are actively forming stars in their bulges. The reason for selecting this sample is threefold. (i) Even though imaged quasar hosts are consistent with being massive ellipticals (e.g. Dunlop et al. 2003), there is some observational evidence that, at high redshift, quasars might be associated with active star formation (e.g. Omont et al. 2001; Hutchings et al. 2002). (ii) In the

[8] Note that equation (18) is more general than the commonly used $N(M) = (M/M_1)^{\alpha}\,\Theta(M - M_0)$ which, for $\alpha = 0$, automatically implies $N(M) = 1$ at any $M > M_0$.

local Universe, powerful Type 2 active galactic nuclei (AGN) are found in bulges with either ongoing star formation or young stellar populations (Kauffmann et al. 2003). (iii) The observed correlation between black hole mass and bulge velocity dispersion suggests that quasar activity and bulge formation probably are physically associated phenomena. For instance, galaxy interactions and bar-induced inflows might funnel some gas into the nuclear region of a galaxy, thereby triggering simultaneous star formation and quasar activity.

Our results show that the halo occupation number of the simulated galaxies is well approximated by a power law with a rather sharp cut-off at low masses. This provides additional motivation to use equation (18) in our analysis.

3.4 Constraints from large-scale clustering

Assuming equation (18), we apply a least-squares method to determine the values of M_0 and α which best describe the clustering data presented in Fig. 1. As discussed in Section 2.5, we use a principal component analysis of the errors to deal with the clustering data. We only consider the region of parameter space where $\alpha \geqslant 0$ and $M_0 \geqslant 10^9$ M$_\odot$. We impose this lower limit to α because we expect the halo occupation number to be a non-decreasing function of the halo mass.[9] On the other hand, we assume a lower limit for M_0 because it is unreasonable to consider halo masses which are smaller than the minimum inferred mass of the black holes powering our quasars (see Appendix A4). In the range of separations covered by our data set ($r \gtrsim 2\,h^{-1}$ Mpc), the two-halo term dominates the amplitude of the quasar two-point correlation function and there is no need to specify the form of the function $\Sigma^2(M)$. From equation (15), we also note that the quasar correlation function on large scales does not depend on the overall normalization of $N(M)$ (e.g. the parameter N_0).

Contour plots of the χ^2 function are shown in Fig. 3. Note that, independently of the redshift interval, the region of parameter space allowed by the data is rather large and does not provide tight constraints on the values of M_0 and α. This is because our data only fix the normalization of the correlation function (e.g. the bias parameter shown in Fig. 2) and there is a whole one-dimensional family of (α, M_0) pairs which correspond to the same clustering amplitude.

3.5 Constraints from the number density

In the halo model described by equation (18), the number density of quasars depends on all the free parameters α, M_0 and N_0. In particular, N_0 acts as an overall normalizing factor so that, for given values of α and M_0, it can be expressed in terms of the mean number density of quasars by combining equations (11) and (18). This gives an additional relationship among the parameters of the model as, for every (α, M_0) pair, there is always a value of N_0 which exactly matches $n_{\rm QSO}$. The dashed lines in Fig. 3 show the regions in the (α, M_0) plane where the observed density corresponds to a given value of $\log_{10} N_0$ (indicated by the labels in the plot). The parameters N_0 and M_0 are strongly covariant; in order to obtain the right

[9] Note that solutions with $\alpha < 0$ are allowed by the data if $M_0 \sim 10^{12.5-13}$ M$_\odot$ (the precise value slightly depending on the assumed redshift range). In this case, quasars are hosted by haloes lying in a narrow mass range which is centred around the values of M_b given in Table 2. For this reason, there is no need to rediscuss these solutions here.

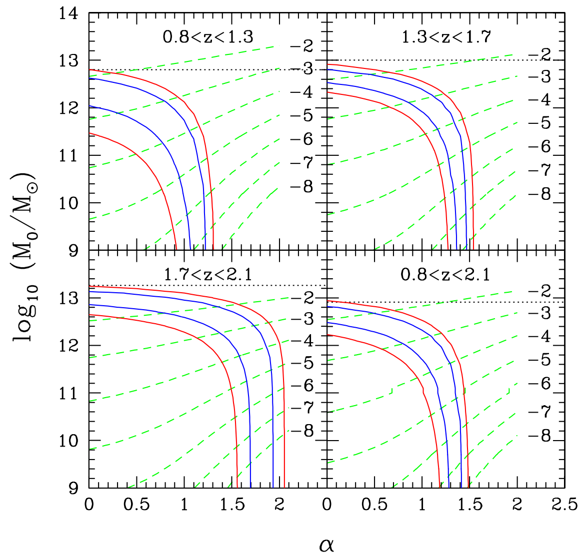

Figure 3. Contour levels of the χ^2 function for the parameters α and M_0 obtained by fitting the large-scale clustering of quasars in different redshift intervals with the predictions of the halo model given in equation (18). The various panels contain contour plots for the χ^2 surface in the α –M_0 plane. The contours correspond to $\Delta\chi^2 = \chi^2 - \chi^2_{\rm min} = 1$ and 4 (respectively marking the 68.3 and 95.4 per cent confidence levels for two fully degenerate Gaussian variables). Contours of the value of $\log_{10} N_0$ which matches the observed number density are plotted as a function of α and M_0 (dashed lines with labels) for the different redshift bins considered. The dotted lines mark the halo masses which correspond to the observed clustering amplitudes (see Table 2).

quasar abundance, we need to lower the normalization of the halo occupation number when M_0 is reduced. The allowed range for N_0 spans many orders of magnitude, reflecting the steep slope of the halo mass function at the low-mass end.

3.6 Constraints from small-scale clustering

For separations smaller than the typical size of the host haloes, the galaxy two-point correlation function is dominated by the contribution of pairs lying within a single halo. In this regime, $\xi(r)$ is fully described by equation (13) which encodes information on the halo occupation distribution through its second factorial moment, $\Sigma^2(M)$. This function can be conveniently expressed in terms of the halo occupation number as follows:

$$\Sigma^2(M) = \Gamma(M)\, N(M)^2. \qquad (19)$$

For a Poisson distribution, $\Gamma(M) = 1$ independently of M. In this case, measuring the two-point correlation function on small scales provides additional constraints on the halo occupation number.

However, in general, the halo occupation distribution function is not Poissonian and $\Gamma(M)$ depends on the halo mass. In principle, this complicates the estimate of $N(M)$ from analyses of small-scale clustering. In fact, a number of additional free parameters might be required to describe the behaviour of $\Gamma(M)$. On the other hand, though, models of galaxy formation suggest that, independently of the galaxy sample considered, $\Gamma(M)$ is a very simple function which can be parametrized in terms of the same variables that are used to describe $N(M)$. Consistent results have been obtained for low-redshift galaxies by using different semi-analytical models (e.g. Sheth & Diaferio 2001; Berlind & Weinberg 2002) and hydrodynamical simulations (Berlind et al. 2003). Similarly, in Appendix B, we use a publicly available semi-analytical model to study the function $\Gamma(M)$ for star-forming galaxies at $z \simeq 1$. In all cases, the scatter of $P_N(M)$ is strongly subPoissonian for haloes which, on average, contain less than one object, and nearly Poissonian for larger haloes. This property plays a fundamental role in breaking the degeneracy among all the models for the halo occupation number which can otherwise accurately describe galaxy clustering on large scales (Magliocchetti & Porciani 2003).

We do not know whether the same conclusions apply to quasars. It is anyway interesting to understand what this would imply. Let us assume that, also for quasars, $\Gamma \ll 1$ when $N \ll 1$ while $\Gamma \simeq 1$ when $N \gtrsim 1$. Within the allowed parameter range in Fig. 3, this implies that, at variance with galaxies, the one-halo term never dominates the quasar correlation function even on scales which are much smaller than the typical halo size. This happens because the quasar $N(M)$ is always much smaller than unity and its associated scatter is strongly subPoissonian. In other words, the distribution of (optically bright) quasars in a halo is binary (either there is one or there is none) and it is basically impossible to find two quasars being hosted by the same halo.

From the absence of quasar multiplets in a single halo it follows that, in order to use observational determinations of quasar clustering on small scales to break the degeneracy among models which predict the same clustering amplitude on large scales, we have to rely on the detection of halo exclusion effects (different haloes cannot overlap). Note that this would be a direct 'measure' of the spatial dimension of dark matter haloes and therefore of their mass.

The exact signature induced by spatial exclusion is hard to predict because dark matter haloes are expected to be triaxial objects and the precise form of the quasar correlation function on small scales is also expected to depend on the position of each quasar within its host halo (see equation 13). However, it is clear that the configuration which maximizes this effect is obtained when quasars sit at the centre of the haloes. In this case, the distribution of quasars is a perfect (sparse sampled) tracer of the underlying halo distribution and the two-point correlation function, $\xi(r)$, is expected to reach the value -1 on scales smaller than the typical size of the host halo. Such exclusion effects will then correspond to a flattening of the projected function Ξ on the same scales. However, these effects might be hard to detect due to the small number statistics of close quasar pairs (see Fig. 1).

Similar arguments apply to any population of rare objects. A possible detection (with relatively low statistical significance) of exclusion effects has been reported from the analysis of the clustering properties of Lyman-break galaxies at redshift $\sim$3 (Porciani & Giavalisco 2002).

Note, however, that the scatter of the halo occupation distribution might depend on the detailed physical processes which give rise to the quasar phenomenon and might thus be very different from the Γ function which describes the galaxy distribution. Therefore, the presence of quasar multiplets inside single haloes is not ruled out by the data. Measuring the quasar two-point correlation function on separations smaller than $1\,h^{-1}$ Mpc would give a definitive answer to this question.

4 HALO OCCUPATION NUMBER FROM QUASAR LUMINOSITIES

Recent studies of stellar and gas dynamics in local galaxies have revealed a wealth of information on the population of supermassive black holes. The observational evidence for a correlation between the mass of a black hole, $M_{\rm bh}$, and the circular velocity, $v_{\rm c}$, of its host galaxy (Ferrarese 2002; Baes et al. 2003) is one of the most intriguing results. In this section, we use this empirically determined relation ($M_{\rm bh} \propto v_{\rm c}^{4.2}$) to derive the halo occupation number of quasars in the 2QZ. This is obtained by first converting quasar luminosities into a distribution of black hole masses (to which we apply the $M_{\rm bh}-v_{\rm c}$ correlation) and then linking, with minimal assumptions, the circular velocity of the host galaxies to the mass of their dark matter haloes.

4.1 Mass of quasar host haloes

The bolometric luminosity of a quasar and the mass of the accreting black hole can be related as follows

$$\frac{M_{\rm bh}}{{\rm M}_{\odot}} = \frac{1}{\eta}\frac{L_{\rm bol}}{1.26\times10^{38}\,{\rm erg\,s^{-1}}}, \tag{20}$$

where η denotes the ratio between the bolometric luminosity of the quasar and the Eddington luminosity. We use this relation to determine the function $\mathcal{P}(M|M_{b_{\rm J}})$ which gives the conditional probability distribution of the host halo mass, M, for a quasar with given absolute magnitude $M_{b_{\rm J}}$. For ease of reading, we just summarize our calculations here while a detailed presentation of the model is given in Appendix A.

To compute $\mathcal{P}(M|M_{b_{\rm J}})$, we first determine the conditional probability of $M_{\rm bh}$ given $M_{b_{\rm J}}$. This is obtained by combining the most recent bolometric corrections from the B band with an empirically determined distribution of Eddington ratios (McLure & Dunlop 2004). We then use the observed $M_{\rm bh}$–$v_{\rm c}$ relation (Baes et al. 2003) to derive the conditional probability of $v_{\rm c}$ given $M_{b_{\rm J}}$. Eventually, we convert circular velocities into halo masses by assuming that the observed circular velocity and the virial velocity of the host halo are related by $v_{\rm c} = \psi\ \ v_{\rm vir}$ where ψ is a free parameter. Recent lensing studies (Seljak 2002) suggest that, in the mass range of interest, $\psi = 1.4 \pm 0.2$ (case A); alternatively, theoretical arguments based on the estimated low concentration of high-redshift haloes suggest that $\psi \simeq 1$ (case B). These different choices bracket the range of plausible values for ψ (see the detailed discussion in Appendix A).

4.2 Halo occupation number

In this section, we test whether the conditional mass distribution $\mathcal{P}(M|M_{b_{\rm J}})$ is consistent with the quasar clustering data we measured in Section 2.5. By integrating over the luminosity function, $\mathcal{P}(M|M_{b_{\rm J}})$ can be easily turned into the mass function of dark haloes which are quasar hosts:

$$n_{\rm q}(M,z) = \int_{M^{\rm f}_{b_{\rm J}}(z)}^{M^{\rm b}_{b_{\rm J}}(z)} \Phi(M_{b_{\rm J}},z)\,\mathcal{P}(M|M_{b_{\rm J}})\,{\rm d}M_{b_{\rm J}}. \tag{21}$$

The corresponding multiplicity function, $M\ \ n_q(M,z)$, is shown in the left-hand panel of Fig. 4 for different values of z. Independently of redshift, the halo mass distribution per unit logarithmic interval of M peaks around $10^{12.5-13}$ ${\rm M}_{\odot}$; this is the characteristic mass of quasar hosts, whose value is comparable with those listed in Table 2. By then dividing $n_{\rm q}(M,z)$ by the halo mass function, we obtain a new estimate for the halo occupation number

$$N(M,z) = \frac{n_{\rm q}(M,z)}{n(M,z)}. \tag{22}$$

Note that this, in principle, could give rise to a biased estimate of $N(M,z)$. In fact, in a CDM cosmology, each virialized halo contains

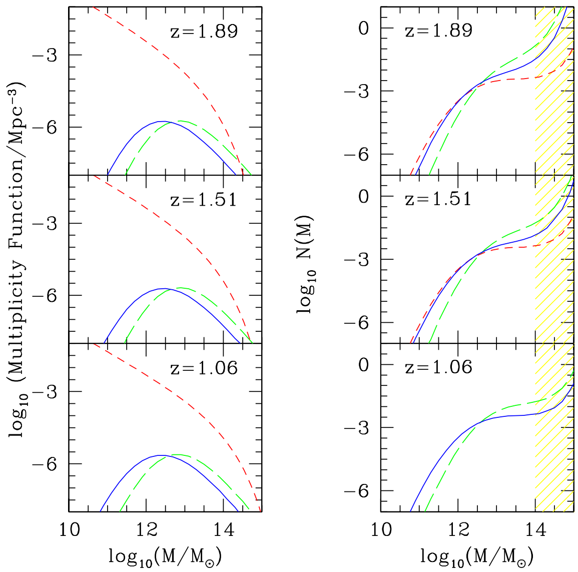

Figure 4. Left-hand panel: the multiplicity function (differential number density per log unit of mass and per unit volume) of haloes which are hosts of 2QZ quasars (solid line for case A, long-dashed line for case B) is compared with the corresponding distribution for all the dark matter haloes (short-dashed line) at different redshifts. Right-hand panel: corresponding halo occupation numbers obtained by taking the ratio of the quasar-host mass function to the total halo mass function (solid line for case A, long-dashed line for case B). For comparison, the case A solution at $z = 1.06$ is reproduced with a short-dashed line in the two top panels.

a number of subhaloes within its $r_{\rm vir}$, and at least some of these subhaloes will be associated with galaxies which formed within their local overdensities and then fell into the larger halo. Because the rotational properties of galaxies are expected to be related to local dark matter overdensities, the values we derived for M most likely refer to subhaloes. On the other hand, $n(M)$ describes the mass distribution of the parent haloes. We can account for this problem by introducing the conditional mass function of the subhaloes of mass $M_{\rm s}$ which lie within a parent halo of mass $M_{\rm p} > M_{\rm s}$, $n(M_{\rm s}|M_{\rm p})$. The probability that a halo with mass M is a parent one is then given by

$$\mathcal{P}_{\rm p}(M) = \frac{n(M)}{n(M) + \int_M^\infty n(M_{\rm p})\, n(M|M_{\rm p})\, {\rm d}M_{\rm p}}, \quad (23)$$

where the integral at the denominator gives the mass function for the subhaloes. We use two different functional forms for $n(M_{\rm s}|M_{\rm p})$ which have been derived from high-resolution numerical simulations (Sheth & Jain 2003; Vale & Ostriker 2004 and references therein). In both cases, we find that the subhalo correction is negligibly small. In fact, at the redshifts spun by our quasar sample, the haloes we are considering are rather massive and only a few per cent of them have been included into larger units.

Results for the halo occupation number are presented in Fig. 4. In all cases, for $M < 10^{14}\ {\rm M}_{\odot}$, $N(M)$ is well approximated by a broken power law which qualitatively resembles equation (18). The low-mass tail has a typical slope ~-3.6 for case A and ~-4.2 for case B, independently of redshift. On the other hand, the high-mass tail becomes progressively steeper when moving from low to high redshifts. For case A, we obtain a flat $N(M)$ for the low-redshift sample, to be compared with a slope of $\sim$0.4 for the data set at intermediate redshifts and of $\sim$0.7 for the highest-redshift quasars. The corresponding numbers for case B are $\sim$0.4, $\sim$0.9 and $\sim$1.1. For $M > 10^{14}\ {\rm M}_{\odot}$, in both cases the halo occupation number starts growing exponentially. This happens because, in the high-mass tail, $n_{\rm q}(M, z)$ does not drop as fast as the exponential cut-off of the halo mass function (see the left-hand panel in Fig. 4 and the shaded region in the right-hand panel). Most likely this is a spurious effect due to the simple assumptions we use to derive $n_{\rm q}(M, z)$. This artefact, however, does not affect our conclusions because the fraction of quasars that are found to reside in such massive haloes is extremely small (at most, a few $\times\ 10^{-5}$ for case A and less than 2 per cent for case B).

Note that estimates for $N(M)$ based on equation (22) are obtained without any information on the clustering properties of quasars. It is therefore interesting to check whether they are in agreement with the determination of $\Xi^{\rm obs}(r_\perp)$ we presented in Section 2.5. For this reason, we compute the effective bias associated with the different halo occupation numbers presented in Fig. 4. For the lowest-redshift sample, we obtain $b_{\rm eff} = 1.63$ (2.02) for case A (B). At intermediate redshifts, we find $b_{\rm eff} = 2.14$ (2.73) for case A (B), while, for the highest-redshift interval, we derive $b_{\rm eff} = 2.58$ (3.36) for case A (B). These numbers have to be compared with the observational results presented in Table 2. For case A, we note that, even though the estimated bias parameter increases with redshift (like the data in Table 2), its value is in general too low to accurately describe the observed clustering. In other words, case A tends to underestimate the mean mass of quasar host haloes. Predictions for case B, instead, are of better quality. In this case, our results for the bias parameter are rather accurate for the intermediate-redshift sample, while they tend to overestimate (underestimate) the observational results at low (high) redshifts. Anyway, the bias inferred from our models is always acceptable (with respect to the statistical errors associated with the determinations of the projected correlation function). The maximum discrepancy appears at $z_{\rm eff} = 1.89$ and corresponds to a statistical significance of 1.4σ. These results are in agreement with the recent analysis by Wyithe & Loeb (2004) who showed that quasar models with $M_{\rm bh} \propto v_{\rm c}^5$, $\psi = 1$ and $\eta \sim$0.1–1 are able to reproduce the evolution of the correlation length measured in a preliminary data release of the 2QZ (Croom et al. 2001, 2002). More accurate clustering measurements are then required to detect possible changes in the $M_{\rm bh}$–$v_{\rm c}$ correlation and to distinguish them from effects due to evolution of other parameters (for instance, η, ψ or the bolometric correction).

5 A BAYESIAN ANALYSIS OF THE HALO OCCUPATION NUMBER

We have shown that, at variance with galaxy clustering, lack of information on (and from) the two-point correlation function of quasars on small scales does not allow us to break the degeneracy among the best-fitting models presented in Fig. 3. In this section, we adopt a Bayesian approach and use information on quasar luminosities to further constrain the parameters of the halo occupation number.

Assuming equation (18), for each redshift interval, we translate the probability density function for the errors of $n_{\rm QSO}$ and $\Xi(r_\perp)$ into a likelihood function for the model parameters and we write

$$\mathcal{L}_{\rm tot}(\alpha, M_0, N_0) = \mathcal{L}_{\rm clust}(\alpha, M_0)\mathcal{L}_{\rm dens}(\alpha, M_0, N_0). \quad (24)$$

Here, $\mathcal{L}_{\rm clust}$ accounts for the large-scale clustering analysis presented in Section 3.4 and $\mathcal{L}_{\rm dens}$ for the quasar number density.[10] In other

[10] Assuming Gaussian errors, $-2\ln\mathcal{L}_i = \chi_i^2 + {\rm const}$ where χ_i^2 denotes the usual χ^2 statistic.

words, the number density constraints weights as much as a single independent point in the clustering analysis. We then apply the Bayes theorem to our data set. For simplicity, to express our lack of prior knowledge, we adopt constant (non-informative) prior distributions for $\log_{10} N_0$ and α. On the other hand, as a prior distribution for $\log_{10}(M_0/\mathrm{M}_\odot)$, we use the probability distribution $\mathcal{P}(M_0|M_{b_\mathrm{J}}^{\max})$, which we have presented in Section 4.1 and derive in Appendix A. This is the probability distribution of the halo masses which harbour the faintest quasars that can be detected in each 2QZ sample considered. This prior knowledge is based on the empirically determined correlation between black hole masses and the circular velocity of the host galaxies. As previously discussed, to test the robustness of our method with respect to underlying systematic uncertainties, we consider two different prior distributions corresponding to $\psi = 1.4 \pm 0.2$ (prior A) and $\psi = 1$ (prior B).

Contours of the posterior probability in the α–M_0 plane and the probability distribution of the single parameters (marginalized over the remaining ones) are shown in Fig. 5. The corresponding best-fitting values and credibility intervals for the different parameters are listed in Table 3.

Note that adopting our informative prior on M_0 is enough to break the degeneracy among the parameters of the best-fitting models. In practice, both priors exclude the region $M_0 < 10^{11}\ \mathrm{M}_\odot$ where haloes are too small to harbour bright quasars. This is sufficient to determine a non-degenerate solution for each redshift range. The main characteristics of these solutions can be summarized as follows. In general, the cut-off mass, M_0, has a very mild evolution with redshift. Using prior A, we obtain $M_0 \sim (1\text{–}3) \times 10^{12}\ \mathrm{M}_\odot$, while, with prior B, we obtain $M_0 \sim (2\text{–}5) \times 10^{12}\ \mathrm{M}_\odot$.[11] On the other hand, in order to match the rapidly evolving bias parameter of the three quasar samples with a nearly invariant M_0, the high-mass slope, α, tends to become steeper and steeper with increasing z. This is in qualitative agreement with the results presented in Section 4.2. At $z_{\mathrm{eff}} = 1.06$, 1.51 and 1.89, we respectively find $\alpha \sim 0.5$, 0.8 and 1.4 for prior A, and $\alpha \sim 0.4$, 0.6 and 1.1 for prior B. It is important to stress, however, that the parameter α is typically poorly determined. Strictly speaking, the data just set an upper limit for it. The allowed range for the normalization parameter N_0 varies systematically with the assumed prior. In brief, N_0 spans a broader range (approximately from 3×10^{-5} to 2×10^{-2}) when prior A is used. On the other hand, with prior B, the probability distribution for N_0 is more peaked and ranges from 3×10^{-4} to 3×10^{-2}. We note that, for both priors, N_0 is less tightly determined for our high-redshift subsample.

6 QUASAR LIFETIME

The number of optically bright quasars per halo can be used to estimate the duty cycle of quasar activity and, thus, the quasar lifetime (Haiman & Hui 2001; Martini & Weinberg 2001). In brief, let us assume, for simplicity, that each dark matter halo contains one supermassive black hole. In this case, the fraction of active quasars per halo coincides with the quasar duty cycle. Assuming that quasar activity is randomly triggered (for instance, by tidal interactions with neighbours) during the halo lifetime, t_{H}, the duty cycle can then be expressed as $t_{\mathrm{Q}}/t_{\mathrm{H}}$ where t_{Q} denotes a characteristic time-scale over which the quasar is visible in the optical band. Both a single optically bright phase and a series of shorter bursts correspond to the same t_{Q}.

[11] Note that M_0 is only mildly covariant with the high-mass slope, α, in the sense that slightly lower values for M_0 are generally associated with larger values of α.

6.1 Estimating the quasar lifetime

In this section, we use the posterior probability distribution presented in Fig. 5 to determine the characteristic quasar lifetime. For each halo mass, we first compute the probability density function of the halo occupation number:

$$\mathcal{P}(N) = \int \delta[N - N(M;\theta)]\, P(\theta|\boldsymbol{D})\, \mathrm{d}^3\theta. \quad (25)$$

where $\delta(x)$ denotes the Dirac-delta distribution, $\theta \equiv (\alpha, M_0, N_0)$, $P(\theta\,|\,\boldsymbol{D})$ is the posterior probability and $N(M;\theta)$ is given in equation (18). The 5, 50 and 95 percentiles of this distribution are shown in Fig. 6 as a function of the halo mass. Note that results are nearly independent of the considered prior. For haloes with $M \simeq 10^{13}\ \mathrm{M}_\odot$, the occupation number is tightly constrained by the data. We thus estimate the characteristic quasar lifetime by assuming that, for these haloes, $N = t_{\mathrm{Q}}/t_{\mathrm{H}}$. Following Martini & Weinberg (2001), the halo lifetime is defined as the median time interval during which a halo of mass M at redshift z is incorporated into a halo of mass $2M$. This quantity is computed using equation (2.22) of Lacey & Cole (1993).

The results for t_{Q} are listed in Table 3. We find that the estimated quasar duty cycle increases with z (and/or with quasar luminosity). For our sample at $z_{\mathrm{eff}} = 1.06$, we find that only ~0.6 per cent of the host haloes with $M = 2 \times 10^{12}\ \mathrm{M}_\odot$ contain a bright quasar, which corresponds to $t_{\mathrm{Q}} \simeq 2 \times 10^7$ yr. This coincides with the e-folding time of a black hole which accretes mass with a radiative efficiency $\epsilon \sim 0.1$ and shines at a fraction $\eta \sim 0.5$ of its Eddington luminosity (Salpeter 1964). On the other hand, at $z_{\mathrm{eff}} = 1.89$, the fraction of active black holes increases to ~5 per cent and $t_{\mathrm{Q}} \simeq 7 \times 10^7$ yr. In all cases, the estimated lifetime lies between 10^7 and 10^8 yr.

Even though the determination of $N(M)$ becomes more uncertain for $M \gg 10^{13}\ \mathrm{M}_\odot$, our results suggest that the occupation number of quasars tends to increase with the halo mass. However, this does not imply that t_{Q} augments as well. In fact, our estimates for the quasar lifetime are degenerate with the occupation number of supermassive black holes which, most likely, increases with the halo mass.

Note that, given the simplicity of the model, our results are only indicative. The quoted quasar lifetimes should be revised upwards if: (i) a non-negligible number of haloes do not harbour any supermassive black hole; (ii) optical radiation from quasars turns out to be significantly beamed; (iii) in the presence of an important fraction of obscured sources. On the other hand, t_{Q} is smaller than that reported here if more than one supermassive black hole is hosted, on average, by each halo.

A number of observations hint towards a one-to-one correspondence between supermassive black holes and host haloes. High-resolution optical imaging with the *Hubble Space Telescope* shows that bright quasars ($M_V < -23$) at $z < 0.5$ are only harboured by exceptionally luminous galaxies with $L \gtrsim L_V^*$ (Bahcall et al. 1997; Hamilton, Casertano & Turnshek 2002). These galaxies turn out to be a mixture of different morphological types, ranging from normal ellipticals and spirals to complex systems of gravitationally interacting components (Bahcall et al. 1997). However, a number of observational results suggest that spheroidal hosts become more prevalent with increasing nuclear luminosities: quasars with $M_V < -23.5$ are virtually all harboured by luminous elliptical galaxies (Dunlop et al. 2003). Similarly, observed surface-brightness

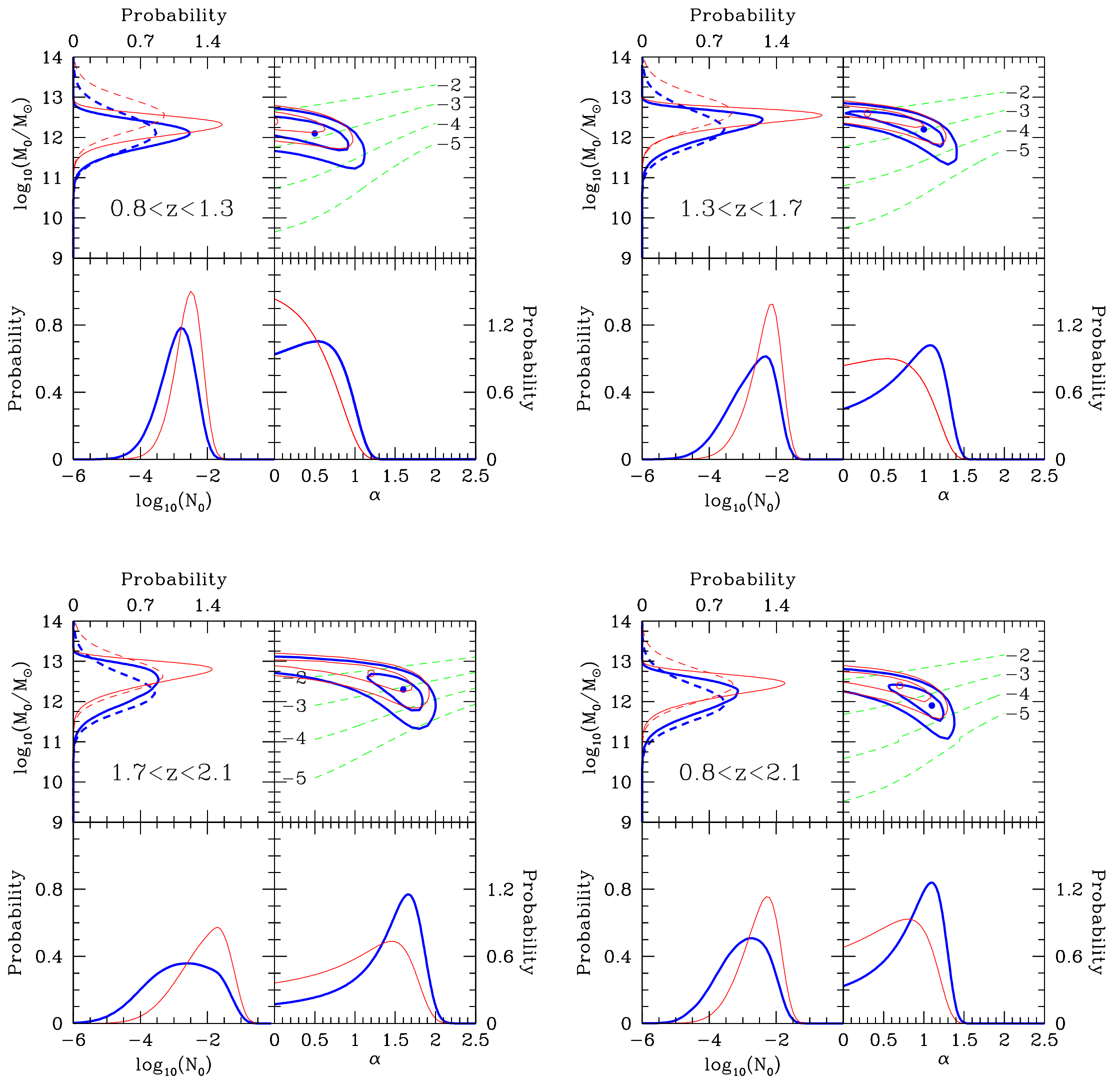

Figure 5. Posterior probability distribution for the parameters of the halo model. The four frames correspond to different redshift ranges as indicated by the labels. Thick and thin lines respectively refer to priors A and B. Top right-hand panel: contours of the joint distribution of α and M_0 (obtained by marginalizing the three-dimensional posterior probability over N_0). The most probable point is marked with a small circle. To facilitate the comparison with Fig. 3, the solid lines show the points where $-0.5\ \ln\ P_{\max}/P = 1$ and 4 (which, in this case, do not have any special meaning). As in Fig. 3, in order to represent the covariance of the different parameters, the dashed lines show the loci in the (α, M_0) plane where a given value of $\log_{10}N_0$ (indicated by the labels) perfectly matches the observed number density of quasars. Other panels: the probability densities for each single parameter (obtained by marginalizing the posterior distribution over the remaining two variables) are shown in the top left-hand (for $\log_{10}M_0/\ \mathrm{M}_{\odot}$), bottom left-hand (for $\log_{10}N_0$) and bottom right-hand (for α) panels. In the top-left-hand panels, the dashed lines show the assumed prior distributions for M_0.

profiles suggest that bright quasars at $z \sim 1$–2 are hosted by massive ellipticals undergoing passive evolution (Kukula et al. 2001; Falomo et al. 2004).[12] Taking this for granted, we can show that our assumption of one supermassive black hole per halo (and thus our inferred quasar lifetime) is rather realistic. The argument proceeds as follows. (i) Massive elliptical galaxies are made of old stellar populations which formed at $z \gtrsim 2$ and passively evolved thereafter. (ii) In the assumed cosmology, the massive haloes which harbour these galaxies can only increase their mass by a factor of a few from $z = 1$–2 to the present epoch. This mainly happens via accretion of smaller objects. (iii) From clustering studies in the local Universe, we derive that haloes with $M \sim 10^{13-14}\ \mathrm{M}_{\odot}$ harbour on average ∼1–2 early-type galaxies with effective luminosity $L_{\mathrm{eff}} = 1.3\ L^*$ (Magliocchetti & Porciani 2003). Points (i), (ii) and (iii) imply that the mean number of early-type galaxies per halo was of order unity even at $z \sim 1$–2. Thus, our thesis follows from the assumption that each galaxy hosts a single supermassive black hole.

[12] Some authors, however, find that a disc-like component is always needed to accurately fit the data at large radii (Percival et al. 2001; Hutchings et al. 2002).

6.2 Constraints from the proximity effect

A quasar produces enhanced ionization of H and He in its surroundings, thus creating opacity gaps in its spectrum (or in the spectrum of background QSOs lying on adjacent lines of sight). The physical characteristics of these H II and He III regions can be used to estimate

Table 3. Best-fitting values for the parameters of the halo model for different redshift ranges (superscript bf). The last three columns list the central 68.3 per cent credibility intervals for each single parameter. These have been obtained by marginalizing the posterior probability distribution function over the remaining parameters. The quoted values correspond to the 15.85, 50 and 84.15 percentiles. In the last column, we list the central 90 per cent credibility intervals for the quasar lifetime. We assume that a halo of 2×10^{13} $M_\odot$ harbours, on average, a single supermassive black hole so that the halo occupation number of bright quasars coincides with their duty cycle.

z_{min}	z_{max}	Prior	$\log_{10}(M_0^{bf}/ M_\odot)$	α^{bf}	$\log_{10} N_0^{bf}$	$\log_{10}(M_0/ M_\odot)$	α	$\log_{10} N_0$	$t_Q/10^7$ yr
0.8	1.3	A	12.1	0.5	−2.9	$12.1^{+0.3}_{-0.4}$	$0.5^{+0.3}_{-0.3}$	$-2.9^{+0.4}_{-0.6}$	$1.9^{+1.8}_{-1.3}$
0.8	1.3	B	12.4	0.0	−2.3	$12.2^{+0.2}_{-0.3}$	$0.4^{+0.3}_{-0.3}$	$-2.6^{+0.3}_{-0.5}$	$2.3^{+1.9}_{-1.4}$
1.3	1.7	A	12.2	1.0	−3.0	$12.3^{+0.3}_{-0.4}$	$0.8^{+0.4}_{-0.5}$	$-2.7^{+0.6}_{-0.8}$	$3.2^{+1.7}_{-1.6}$
1.3	1.7	B	12.6	0.3	−2.1	$12.5^{+0.2}_{-0.3}$	$0.6^{+0.4}_{-0.4}$	$-2.3^{+0.3}_{-0.6}$	$3.2^{+2.3}_{-1.5}$
1.7	2.1	A	12.3	1.6	−3.1	$12.4^{+0.4}_{-0.5}$	$1.4^{+0.4}_{-0.7}$	$-2.8^{+1.0}_{-1.1}$	$5.9^{+5.3}_{-2.4}$
1.7	2.1	B	12.7	1.2	−2.1	$12.7^{+0.3}_{-0.4}$	$1.1^{+0.5}_{-0.7}$	$-2.1^{+0.7}_{-0.8}$	$6.8^{+7.3}_{-2.9}$
0.8	2.1	A	12.0	1.0	−3.1	$12.1^{+0.3}_{-0.4}$	$0.8^{+0.3}_{-0.5}$	$-2.8^{+0.6}_{-0.8}$	$3.0^{+2.2}_{-1.8}$
0.8	2.1	B	12.4	0.5	−2.2	$12.3^{+0.2}_{-0.3}$	$0.6^{+0.4}_{-0.4}$	$-2.4^{+0.4}_{-0.6}$	$3.2^{+2.6}_{-1.9}$

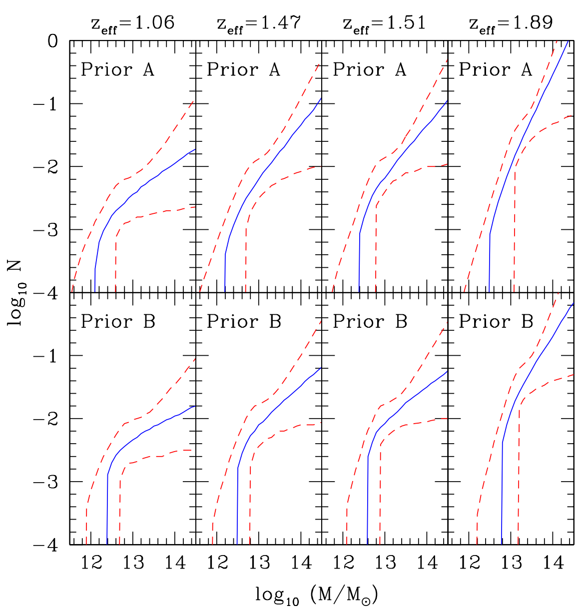

Figure 6. Halo occupation number obtained from the posterior probability distribution in Fig. 5. For each halo mass, M, we derive the probability density function of N using equation (25). Solid lines show the median occupation number as a function of M while dashed lines indicate the 5 and 95 percentiles of the distribution.

the quasar lifetime (e.g. Bajtlik, Duncan & Ostriker 1988; Heap et al. 2000). A number of studies have shown that, in order to explain the proximity effect in the Ly-α forest, quasars have to maintain their ionizing luminosity for at least 10^5 yr (e.g. Bajtlik, Duncan & Ostriker 1988; Schirber, Miralda-Escudé & McDonald 2004). At the same time, the best estimates for the quasar lifetimes indicate that $t_Q \gtrsim 10^7$ yr (Hogan, Anderson & Rugers 1997; Anderson et al. 1999; Jakobsen et al. 2003). It is interesting to check what are the implications of these observational results for our halo model. We first note that extremely short quasar lifetimes correspond to very low values for N_0. From Fig. 3, we then learn that the condition $t_Q > 10^5$ yr basically rules out all the models with $M_0 \lesssim 10^{11}$ $M_\odot$. On the other hand, a time-scale $\gtrsim 10^7$ yr is fully consistent with our results for t_Q presented in Section 6. In other words, constraints on the halo model from quasar luminosities and from the proximity effect are consistent and approximately equivalent. Future determinations of quasar radiative histories based on the transverse proximity effect (e.g. Adelberger 2004 and references therein) will hopefully provide more stringent limits.

7 IS THE HALO OCCUPATION NUMBER EVOLVING?

The analysis presented in Section 3 is based on two basic assumptions: the halo model and an assumed functional form for $N(M)$, i.e. equation (18). Within these working hypotheses, in the three-dimensional parameter space (α, M_0, N_0) we have identified a one-dimensional family of models which accurately fits the abundance and clustering properties of quasars in the 2QZ. Prior information on M_0, inferred from quasar luminosities, was used in Section 4 to remove the degeneracy between the model parameters.

In this section, we want to test whether quasar clustering (without any additional constraint from quasar luminosity) is consistent with a non-evolving model for $N(M)$. Indeed, the contours in Fig. 3 obtained for quasars at different redshifts tend to lie in the same region of the α–M_0 parameter space. This also applies to the halo occupation number of the entire quasar sample ($0.8 < z < 2.1$). We then assume, as a working hypothesis, that the shape of the halo occupation number (parametrized by α and M_0) does not evolve within the time interval spun by our quasar data set. On the other hand, we let the overall normalization N_0 vary. In fact, because of selection effects, quasars lying at higher redshifts tend to be (on average) intrinsically brighter than their lower-redshift counterparts

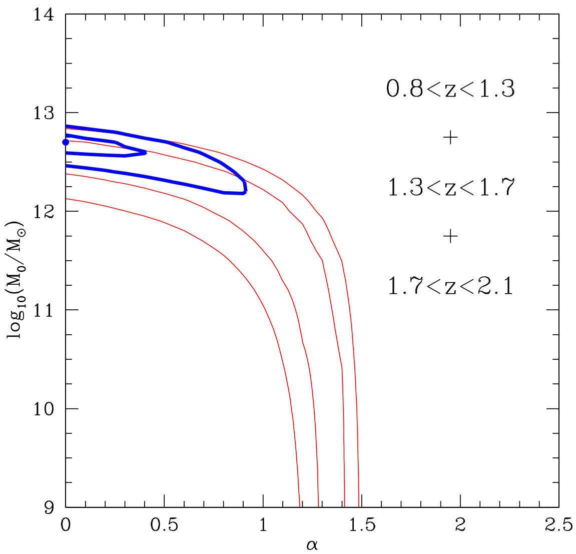

Figure 7. Contour levels for the χ^2 function obtained by combining the quasar subsamples at different redshifts and assuming that the shape of the halo occupation number does not evolve with z. The χ^2 function is shown as a function of the halo model parameters α and M_0 and it has been minimized with respect to $N_0^{\rm L}$, $N_0^{\rm M}$ and $N_0^{\rm H}$. A point indicates the best-fitting model while the heavy lines mark the 68.3 and 95.4 per cent confidence levels (respectively corresponding to $\Delta\chi^2 = 2.3$ and 6.17). For ease of comparison, the contours presented in the bottom-right-hand panel of Fig. 3 are represented with light lines. These refer to the halo occupation number of our entire quasar sample in the redshift range $0.8 < z < 2.1$.

(see Table 1). Therefore, because we are considering objects within different luminosity ranges, it is reasonable to assume that they will correspond to different values of N_0 and, thus, to different number densities. We denote these new parameters as $N_0^{\rm L}$, $N_0^{\rm M}$ and $N_0^{\rm H}$, respectively, for the low-, median- and high-redshift samples.

In Fig. 7, we show the confidence levels in the (α, M_0) plane obtained by combining the three redshift subsamples. The objective function (total χ^2) has been computed by adding together the χ^2 of each sample. The contours shown in the figure are obtained by minimizing the total χ^2 function over the different N_0^i (we remind the reader that for each pair of values for (α, M_0) it is always possible to choose the N_0^i so as to perfectly match the observed densities).

The minimum value assumed by the total χ^2 function over the parameter space is 10.98 with 10 degrees of freedom. Therefore, assuming Gaussian errors, our working hypothesis that the halo occupation number of bright quasars does not evolve with redshift is not rejected by the data at any significant confidence level. The best-fitting values for the parameters are $\alpha = 0.0^{+0.4}$, $M_0 = 12.7 \pm 0.1$, $\log_{10} N_0^{\rm L} = -1.96^{+0.14}_{-0.26}$, $\log_{10} N_0^{\rm M} = -1.86^{+0.15}_{-0.24}$ and $\log_{10} N_0^{\rm H} = -1.73^{+0.17}_{-0.27}$. All the quoted intervals correspond to $\Delta\chi^2 = 1$. This corresponds to $b_{\rm eff} = 2.08 \pm 0.10$, 2.64 ± 0.15 and 3.20 ± 0.20, respectively, for the low-, medium- and high-redshift samples. In this case then, changes in the bias parameter are merely driven by the joint time evolution of the halo population and of the mass autocorrelation function.

In summary, the combined data set is consistent with a model for the halo occupation number which does not evolve with look-back time and exhibits a very shallow dependence on the halo mass ($\alpha < 1$, with values near zero which are favoured). We also find $M_0 \simeq 5 \times 10^{12}$ M$_\odot$ and $N_0^i \simeq 0.01$–0.02. For all the quasar subsamples, this corresponds to $t_{\rm Q} \simeq (3$–$4) \times 10^7$ yr.

8 DISCUSSION

8.1 Comparison of results

In Sections 4.2, 5 and 7 we derived the quasar halo occupation number using a few different methods. The corresponding outcomes are fully consistent with each other. In all cases, we find that bright quasars are hosted by massive haloes with $M \gtrsim 10^{12}$ M$_\odot$. For larger halo masses, the shape of the halo occupation number is not well constrained by the observational data and a wide range of possibilities is allowed. However, independently of the model details, we find that quasar hosts have characteristic masses of a few $\times\ 10^{13}$ M$_\odot$. This is the key result of this analysis which strongly constrains quasar formation models. For instance, by coupling hydrodynamical simulations of galaxy formation with simple recipes for AGN activation, Di Matteo et al. (2003) recently concluded that quasar hosts at $z \sim 2$ have typical masses of $\sim 4 \times 10^{12}$ M$_\odot$. The corresponding clustering amplitude ($b \sim 1.6$ at $z = 1.89$) is too low to match our measures ($b = 3.9 \pm 0.3$ at $z_{\rm eff} = 1.89$), thus suggesting that some revision of the model is probably required.

On the other hand, our findings are in good agreement with the typical mass of haloes hosting local radio galaxies (Magliocchetti et al. 2004). This further strengthens the connection between AGN which exhibit different observational properties.

8.2 Control of systematics

A number of assumptions have been used in the present study. We discuss here how possible sources of systematic errors might affect our results.

All our analysis is developed within a specified cosmological framework based on the CDM paradigm. Modifying the cosmological parameters within the ranges allowed by recent CMB studies (e.g. Tegmark et al. 2004) induces minor changes in our conclusions. Results similar to those presented here are also obtained by slightly altering the power spectrum of density fluctuations. For instance, neglecting the presence of baryons (i.e. modifying the shape parameter of the linear power spectrum from 0.16 to 0.21) increases the bias parameters of our subsamples by ∼7 per cent. In consequence, our best-fitting values for α increase by 0.2–0.3. At the same time, for a given α, the best-fitting values for $\log_{10} M_0$ and $\log_{10} N_0$ increase by 0.2–0.4.

The normalization of the linear power spectrum of density fluctuations is still very controversial: estimates of σ_8 from weak lensing and cluster abundances range between 0.7 and 1 (see, for example, table 4 in Tegmark et al. 2004 for a list of the most recent determinations). In Table 4, we use our entire sample of quasars to show how the best-fitting parameters of the halo model change with σ_8. For simplicity, we just consider models with $\alpha = 0$ and $\alpha = 1$. Note

Table 4. Dependence of the best-fitting bias and halo model parameters on σ_8. The first set of data refers to models with $\alpha = 0$ and the second to $\alpha = 1$. The entire quasar sample ($0.8 < z < 2.1$) is considered here.

σ_8	b	$\log_{10}\frac{M_0}{\rm M_\odot}$ ($\alpha = 0$)	$\log_{10} N_0$ ($\alpha = 0$)	$\log_{10}\frac{M_0}{\rm M_\odot}$ ($\alpha = 1$)	$\log_{10} N_0$ ($\alpha = 1$)
0.7	2.76 ± 0.23	$12.5^{+0.1}_{-0.2}$	$-1.8^{+0.2}_{-0.3}$	$12.0^{+0.2}_{-0.4}$	$-2.9^{+0.3}_{-0.5}$
0.8	2.42 ± 0.20	$12.6^{+0.1}_{-0.2}$	$-1.8^{+0.2}_{-0.3}$	$12.0^{+0.2}_{-0.4}$	$-3.1^{+0.3}_{-0.5}$
0.9	2.15 ± 0.18	$12.6^{+0.1}_{-0.2}$	$-1.9^{+0.2}_{-0.3}$	$11.9^{+0.2}_{-0.4}$	$-3.3^{+0.3}_{-0.5}$
1.0	1.91 ± 0.16	$12.7^{+0.1}_{-0.2}$	$-1.9^{+0.2}_{-0.3}$	$11.7^{+0.2}_{-0.4}$	$-3.6^{+0.4}_{-0.6}$

that, while the estimated bias parameter and σ_8 are inversely proportional, the best-fitting parameters of the halo model depend only slightly on the assumed value for σ_8 (compared with their statistical uncertainty).

Our analysis relies on a set of fitting functions calibrated against numerical simulations. These have been used to compute the mass function and bias parameter of dark matter haloes and the non-linear power spectrum of density fluctuations. Considering all the uncertainties, we estimate that, on the scales considered here, the accuracy of the resulting correlation function is of the order of 10–20 per cent. This is still smaller than the statistical error associated with the observed correlation function. Consequently, we do not expect our results to be significantly affected by this source of systematic errors.

We used the most recent observational determinations of the Eddington ratio and of the correlation between $M_{\rm bh}$ and $v_{\rm c}$ to estimate the mass function of quasar host haloes. What is the sensitivity of our results to these assumptions? Assuming that all high-redshift quasars shine at the Eddington luminosity (which is slightly extreme but certainly plausible) would decrease our estimates for $M_{\rm bh}$ by a factor of 2–3 and the mass of the host haloes by a factor of 3–5. The best-fitting solutions for $N(M)$ would then correspond to values for α that are slightly larger than those presented in Section 4.

A large fraction of quasar-host galaxies are morphologically disturbed or interacting. This suggests that efficient black hole fuelling is triggered by galaxy encounters involving at least one gas-rich object. Based on this, Kauffmann & Haehnelt (2000) developed a merger-based prescription of AGN activation. In our analysis, we never distinguish between merging and non-merging haloes. Can this bias our results? Previous studies have shown that, at $z \sim 2$, merging and randomly selected haloes of the same mass have the same clustering properties (Kauffmann & Haehnelt 2002; Percival et al. 2003). This implies that our results are valid also in the merger-driven scenario for AGN. However, if quasars are indeed found only in merging haloes, our estimates for $t_{\rm Q}$ should be revised upwards by a factor of $f_{\rm mer}^{-1}$ where $f_{\rm mer}$ is the fraction of merging haloes.

8.3 Number density evolution: implications for high-redshift quasars

It is interesting to study how the number density of quasars with a given halo occupation number evolves. This is shown, for different halo models, in the left-hand panel of Fig. 8. In all cases, the number density rapidly drops with redshift as a consequence of the hierarchical assembly of dark matter haloes (see also Efstathiou & Rees 1988). On the other hand, by integrating the 2QZ luminosity function (Croom et al. 2004) above a given threshold value, one finds that, between $0.4 < z < 2.1$, $n_{\rm QSO}$ increases with look-back time (see Fig. 8). This is clearly seen also in Table 1: both our low-redshift subsample and our full sample roughly correspond to $M_{b_{\rm J}} < -22.5$ but the quasar number density at $z_{\rm eff} = 1.47$ is a factor of 1.3 higher than at $z_{\rm eff} = 1.06$. We then conclude that, at $z < 2$ and for a given luminosity threshold, the quasar halo occupation number cannot remain constant with time; at least its overall normalization, N_0, (and the corresponding quasar lifetime) has to increase with z. This is probably due to the fast depletion of the gas available for accretion on to supermassive black holes during the late stages of galaxy and group formation (e.g. Cavaliere & Vittorini 2000). Once again, it is important to stress the different nature of the halo model parameters. Basically, while M_0 determines which haloes are capable of hosting supermassive black holes, N_0 and α fix the overall normalization and the scaling of the halo occupation number with the halo mass. These two parameters are probably more influenced (with respect to M_0) by the local physics which determines the efficiency of gas accretion.

It is reasonable to expect that a fixed halo occupation number might accurately describe the quasar density evolution at higher

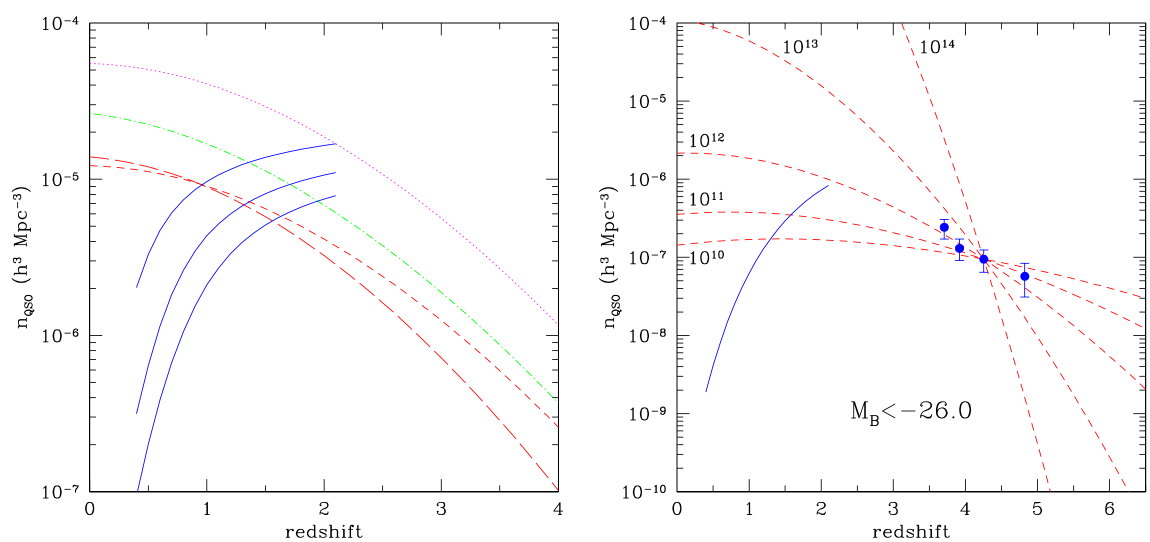

Figure 8. Number density evolution of optically bright quasars. Left-hand panel: the solid lines are obtained using the best-fitting luminosity function from the 2QZ (Croom et al. 2004). From top to bottom, they refer to $M_{b_{\rm J}} < -22.5, -23.6, -24.1$ (which correspond to the faintest objects in our subsamples). The remaining lines show the evolution of $n_{\rm QSO}$ corresponding to a fixed halo occupation number. Two best-fitting models for $N(M)$ at $z_{\rm eff} = 1.06$ are represented with dashed lines: the prior B solution discussed in Section 4 (short-dashed) and the non-evolving model presented in Section 7 (long-dashed). The dot-dashed line shows the best-fitting (prior B) model for our full sample. The dotted line is obtained by renormalizing the short-dashed line so as to fit the 2QZ data at $z = 2.1$ (which corresponds to $\log_{10} N_0 = -1.65$). Right-hand panel: data points with error bars show the high-redshift results from the SDSS Quasar Survey (Fan et al. 2001). The solid lines are obtained using the best-fitting luminosity function from the 2QZ (Croom et al. 2004). The dashed lines refer to halo occupation models of the form $N(M) = N_0\,\Theta(M - M_0)$. The adopted values for M_0 are indicated in the figure and N_0 is fixed so as to match the observed quasar density at $z \sim 4$.

redshifts when gas is ubiquitously available within massive dark matter haloes. In fact, there is a consensus that the comoving number density of optically selected quasars peaks at $z \sim 2$–3 and drops rapidly at higher redshifts.[13] This is naturally explained by CDM models where galaxies form at relatively late times (Efstathiou & Rees 1988). In the right-hand panel of Fig. 8, we compare the density evolution predicted by the halo model with observational data from the 2QZ and the SDSS Quasar Survey (Fan et al. 2001). For simplicity, we set $\alpha = 0$ and we assume that the function $N(M)$ does not evolve with time. We find that models with $M_0 \gtrsim 10^{12}$ M$_\odot$ are consistent with the observed number density of quasars with $M_B <$ 26 in the redshift interval $2 \lesssim z \lesssim 5$. On the other hand, as discussed above, a fixed $N(M)$ cannot match the data at $z < 2$. Similar results are also obtained for a brighter sample of *i*-dropout objects detected at $z \sim 6$ (Fan et al. 2004).

Knowledge of the number density evolution, however, does not provide enough information to determine the nature of high-redshift quasars. In fact, different halo occupation models which are compatible with the observed evolution of $n_{\rm QSO}$ correspond to wildly discrepant quasar characteristics. For instance, at $z = 4$, a model with $\alpha = 0$ and $M_0 = 10^{12}$ M$_\odot$ corresponds to a correlation length of $6.7\,h^{-1}$ Mpc ($b = 5.0$) and to a mean host halo mass of $\langle M \rangle =$ 1.8×10^{12} M$_\odot$. In this case, the observed number density implies that $N_0 = 3.8 \times 10^{-4}$ and $t_{\rm Q} = 2.5 \times 10^5$ yr. Thus, assuming that equation (A4) still holds at $z = 4$, from the estimated $\langle M \rangle$, we derive $M_{\rm bh} = 1.2 \times 10^8$ M$_\odot$, which implies a super-Eddington accretion rate with $\eta = 2.8$. On the other hand, the corresponding results for a model with $\alpha = 0$ and $M_0 = 10^{13}$ M$_\odot$ are $N_0 =$ 0.18, $r_0 = 14\,h^{-1}$ Mpc ($b = 9.2$), $\langle M \rangle = 1.4 \times 10^{13}$ M$_\odot$, $t_{\rm Q} =$ 1.3×10^8 yr, $M_{\rm bh} = 2.1 \times 10^9$ M$_\odot$ and $\eta = 0.16$. This clearly shows that future clustering measurements (hopefully combined with information on $t_{\rm Q}$) will be crucial to understanding the physical properties of high-redshift quasars. The low abundance of optically bright objects, however, poses enormous difficulties for this type of study.

9 SUMMARY

We have used a flux-limited sample of $\sim$ 14 000 2QZ quasars with $M_{b_{\rm J}} < -22.5$ to study the quasar clustering properties in the redshift range $0.8 < z < 2.1$. Our main results are summarized as follows.

(i) For spatial separations between 1 and $20\,h^{-1}$ Mpc, the correlation function for our whole quasar sample (corresponding to an effective redshift $z_{\rm eff} = 1.47$) is well approximated by a power law with slope $\gamma = 1.53 \pm 0.20$ and comoving correlation length $r_0 =$ $4.8^{+0.9}_{-1.5}\,h^{-1}$ Mpc.

(ii) Splitting the sample into three redshift ranges, we find evidence for an increase of the clustering amplitude with look-back time. The correlation function for quasars at $1.7 < z < 2.1$ ($z_{\rm eff} =$ 1.89) is nearly a factor of 2 higher with respect to the whole sample ($z_{\rm eff} = 1.47$). Because flux-limited surveys tend to select intrinsically brighter objects at higher redshifts, it is not possible to tell, however, whether this effect is due to real evolution of the quasar population or to luminosity-dependent clustering. We will further address this issue in a future paper.

[13] A number of factors (namely, observational incompletenesses, uncertainties in the *K*-corrections and the possibility that a large fraction of quasars is not detectable in the optical band due to dust extinction) could generate a spurious drop but it is widely believed that at least part of the observed decrease is real (see, for example, the discussion in Fan et al. 2001).

(iii) For all the subsamples, the correlation function is well approximated by a power law. The best-fitting parameters, which are strongly covariant (see Fig. 1), range between $-2.0 \lesssim \gamma \lesssim$ -1.5 and $4 \lesssim r_0/\ h^{-1}$ Mpc $\lesssim 8$ (see Table 2). Within the statistical uncertainties, data in different redshift bins can be anyway described by the same value of γ. Assuming that the slope of the correlation function does not change with redshift, evolution of the correlation length is detected at the 3.6σ confidence level.

(iv) Within the framework of concordance cosmology, high-redshift quasars are more biased tracers of the mass distribution than their low-redshift counterparts. The observed quasar-to-mass bias parameter is consistent with being scale-independent for the separations probed by our analysis. Assuming $\sigma_8 = 0.8$, we obtain $b = 2.42^{+0.20}_{-0.21}$ for the whole quasar sample. On the other hand, we find $b = 1.80^{+0.20}_{-0.24}$ for $0.8 < z < 1.3$, $b = 2.62^{+0.18}_{-0.19}$ for $1.3 < z <$ 1.7 and $b = 3.86^{+0.32}_{-0.35}$ for $1.7 < z < 2.1$. In hierarchical models for structure formation, the bias parameter of a population of tracers can be readily linked to the mass of their host dark matter haloes. At a given z, values of b which are significantly larger than unity correspond to haloes with $M \gg M_*(z)$ where $M_*(z)$ denotes the characteristic mass of haloes which are forming at that epoch out of 1σ density fluctuations. The bias parameters of our subsamples then suggest that 2QZ quasars are hosted by rare haloes with $M \sim$ 10^{13} M$_\odot$.

(v) Using the halo model, we find that the observed quasar number density and clustering amplitude are consistent with a picture where (i) quasars form in haloes with $M > 10^{12}$ M$_\odot$, and (ii) the characteristic mass of their host haloes is a few $\times 10^{13}$ M$_\odot$. This result is independent of the detailed form of the halo occupation number, and hence it can be used to constrain models of quasar formation.

(vi) Our best-fitting models at $z_{\rm eff} = 1.06$ suggest that $N(M) \propto$ $M^{0.4-0.5}$ for $M > 10^{12}$ M$_\odot$ and rapidly drops to zero for smaller values of M. For higher redshifts, $N(M)$ tends to increase more rapidly with the halo mass. For instance, at $z_{\rm eff} = 1.89$, $N(M) \propto$ $M^{1-1.5}$ for $M > 10^{13}$ M$_\odot$. It is worth stressing, however, that the data are also consistent with a non-evolving functional form for $N(M)$ where quasars reside in haloes more massive than 5×10^{12} M$_\odot$ and where the halo occupation number has a very weak dependence on the halo mass.

(vii) The mean number of quasars per halo is always much smaller than one. Systematic searches for close pairs are needed to understand whether two active quasars can be hosted by a single halo.

(viii) The observed clustering evolution is consistent with assuming that the locally observed correlation between black hole mass and host galaxy circular velocity (Ferrarese 2002; Baes et al. 2003) is still valid at $z > 1$.

(ix) The fraction of potential host haloes which indeed harbour a bright quasar increases from $\lesssim 1$ per cent at $z_{\rm eff} = 1.06$ to 5–10 per cent at $z_{\rm eff} = 1.89$. From this, we infer that the characteristic quasar lifetime $t_{\rm Q}$ increases with redshift (and/or with optical luminosity), ranging from a few $\times 10^7$ yr at $z \sim 1$ to $\sim 10^8$ yr at $z \sim 2$. This is in good agreement with studies of the proximity effect (e.g. Jakobsen et al. 2003 and references therein).

(x) For $z < 2$, the halo occupation number of quasars which are above a given absolute luminosity threshold cannot remain constant with time. In order to match the observed number density evolution, at least its overall normalization N_0 (and thus the corresponding $t_{\rm Q}$) has to increase with z. This probably reflects the fast depletion of the gas available for accretion on to supermassive black holes during the process of galaxy formation.

In brief, this paper presents state-of-the-art measurements of quasar clustering and establishes an accurate benchmark for quasar formation models. Future results from the SDSS Quasar Survey will provide an independent verification of our results and, thanks to the different quasar selection criteria, will extend them to even higher redshifts.

ACKNOWLEDGMENTS

CP and PN thank Simon Lilly for useful suggestions and comments. MM acknowledges Gianfranco De Zotti and Luigi Danese for many clarifying discussions. PN thanks Phil Outram and Tom Shanks for stimulating discussions about the 2QZ. We are grateful to the anonymous referee for valuable suggestions that improved the presentation of our results. CP and PN are supported by the Zwicky Prize fellowship program at ETH-Zürich. The 2QZ was compiled by the 2QZ survey team from observations made with the 2dF on the Anglo-Australian Telescope.

REFERENCES

Adelberger K. L., 2000, in Mazure A., Le Fèvre O., Le Brun V., eds, ASP Conf. Ser. Vol. 200, Clustering at High Redshift. Astron. Soc. Pac., San Francisco, p. 13
Adelberger K. L., 2004, ApJ, 612, 706
Adelberger K. L., Steidel C. C., Shapley A. E., Pettini M., 2003, ApJ, 584, 45
Anderson S. F., Hogan C. J., Williams B. F., Carswell R. F., 1999, AJ, 117, 56
Andreani P., Cristiani S., 1992, ApJ, 398, L13
Andreani P., Cristiani S., Lucchin F., Matarrese S., Moscardini L., 1994, ApJ, 430, 458
Arnouts S., Cristiani S., Moscardini L., Matarrese S., Lucchin F., Fontana A., Giallongo E., 1999, MNRAS, 310, 54
Baes M., Buyle P., Hau G. K. T., Dejonghe H., 2003, MNRAS, 341, L44
Bahcall J. N., Kirhakos S., Saxe D. H., Schneider D. P., 1997, ApJ, 479, 642
Bajtlik S., Duncan R. C., Ostriker J. P., 1988, ApJ, 327, 570
Bechtold J. et al., 1994, AJ, 108, 374
Berlind A. A., Weinberg D. H., 2002, ApJ, 575, 587
Berlind A. A. et al., 2003, ApJ, 593, 1
Blair M., Gilmore G., 1982, PASP, 94, 742
Brotherton M. S., Tran H. D., Becker R. H., Gregg M. D., Laurent-Muehleisen S. A., White R. L., 2001, ApJ, 546, 775
Bryan G. L., Norman M. L., 1998, ApJ, 495, 80
Bullock J. S., Kolatt T. S., Sigad Y., Somerville R. S., Kravtsov A. V., Klypin A. A., Primack J. R., Dekel A., 2001, MNRAS, 321, 559
Bullock J. S., Wechsler R. H., Somerville R. S., 2002, MNRAS, 329, 246
Carlberg R. G., Cowie L. L., Songaila A., Hu E. M., 1997, ApJ, 484, 538
Catelan P., Lucchin F., Matarrese S., Porciani C., 1997, MNRAS, 297, 692
Cavaliere A., Vittorini V., 2000, ApJ, 543, 599
Coil A. L. et al., 2004, ApJ, 609, 525
Cole S., Kaiser N., 1989, MNRAS, 237, 1127
Colless M. et al., 2001, MNRAS, 328, 1049
Corbett E. A. et al., 2003, MNRAS, 343, 705
Cristiani S., Vio R., 1990, A&A, 227, 385
Croom S. M., Shanks T., 1996, MNRAS, 281, 893
Croom S. M., Shanks T., Boyle B. J., Smith R. J., Miller L., Loaring N. S., Hoyle F., 2001, MNRAS, 325, 483
Croom S. M., Boyle B. J., Loaring N. S., Miller L., Outram P. J., Shanks T., Smith R. J., 2002, MNRAS, 335, 459
Croom S. M., Smith R. J., Boyle B. J., Shanks T., Miller L., Outram P. J., Loaring N. S., 2004, MNRAS, 349, 1397
Daddi E., Broadhurst T., Zamorani G., Cimatti A., Röttgering H., Renzini A., 2001, A&A, 376, 825
Di Matteo T., Croft R. A. C., Springel V., Hernquist L., 2003, ApJ, 593, 56
Dunlop J. S., McLure R. J., Kukula M. J., Baum S. A., O'Dea C. P., Hughes D. H., 2003, MNRAS, 340, 1095
Efstathiou G., 1988, in Lawrence A., ed., Proc. 3rd IRAS Conf., Comets to Cosmology. Springer, New York, p. 312
Efstathiou G., Rees M. J., 1988, MNRAS, 230, 5
Elvis M. W. et al., 1994, ApJS, 95, 1
Elvis M., Risaliti G., Zamorani G., 2002, ApJ, 565, L75
Enoki M., Nagashima M., Gouda N., 2003, PASJ, 55, 133
Fabian A. C., Iwasawa K., 1999, MNRAS, 303, L34
Falomo R., Kotilainen J. K., Pagani C., Scarpa R., Treves A., 2004, ApJ, 604, 495
Fan X. et al., 2001, AJ, 121, 54
Fan X. et al., 2004, AJ, 128, 515
Ferrarese L., 2002, ApJ, 578, 90
Ferrarese L., Merritt D., 2000, ApJ, 539, L9
Firth A. E. et al., 2002, MNRAS, 332, 617
Gebhardt K. et al., 2000, ApJ, 539, L13
Granato G. L., De Zotti G., Silva L., Bressan A., Danese L., 2004, ApJ, 600, 580
Grazian A., Negrello M., Moscardini L., Cristiani S., Haehnelt M. G., Matarrese S., Omizzolo A., Vanzella E., 2004, AJ, 127, 592
Haehnelt M. G., Kauffmann G., 2000, MNRAS, 318, 35
Haehnelt M. G., Natarajan P., Rees M. J., 1998, MNRAS, 300, 817
Haiman Z., Hui L., 2001, ApJ, 547, 27
Hamana T., Ouchi M., Shimasaku K., Kayo I., Suto Y., 2004, MNRAS, 347, 813
Hamilton A. J. S., 1993, ApJ, 417, 19
Hamilton T. S., Casertano S., Turnshek D. A., 2002, ApJ, 576, 61
Hatton S., Devriendt J. E. G., Ninin S., Bouchet F. R., Guiderdoni B., Vibert D., 2003, MNRAS, 343, 75
Heap S. R., Williger G. M., Smette A., Hubeny I., Sahu M. S., Jenkins E. B., Tripp T. M., Winkler J. N., 2000, ApJ, 534, 69
Hogan C. J., Anderson S. F., Rugers M. H., 1997, AJ, 113, 1495
Hoyle F., Outram P. J., Shanks T., Croom S. M., Boyle B. J., Loaring N. S., Miller L., Smith R. J., 2002, MNRAS, 329, 336
Hutchings J. B., Frenette D., Hanisch R., Mo J., Dumont P. J., Redding D. C., Neff S. G., 2002, AJ, 123, 2936
Iovino A., Shaver P. A., 1988, ApJ, 330, L13
Jakobsen P., Jansen R. A., Wagner S., Reimers D., 2003, A&A, 397, 891
Kaiser N., 1987, MNRAS, 227, 1
Kauffmann G., Haehnelt M. G., 2000, MNRAS, 311, 576
Kauffmann G., Haehnelt M. G., 2002, MNRAS, 332, 529
Kauffmann G. et al., 2003, MNRAS, 346, 1055
Kukula M. J., Dunlop J. S., McLure R. J., Miller L., Percival W. J., Baum S. A., O'Dea C. P., 2001, MNRAS, 326, 1533
Lacey C., Cole S., 1993, MNRAS, 262, 627
La Franca F., Andreani P., Cristiani S., 1998, ApJ, 497, 529
Landy S. D., Szalay A. S., 1993, ApJ, 412, 64
Le Fèvre O., Hudon D., Lilly S. J., Crampton D., Hammer F., Tresse L., 1996, ApJ, 461, 534
Lynden-Bell D., 1969, Nat, 223, 690
McLure R. J., Dunlop J. S., 2004, MNRAS, 352, 1390
Magliocchetti M., Maddox S., 1999, MNRAS, 306, 988
Magliocchetti M., Porciani C., 2003, MNRAS, 346, 186
Magliocchetti et al., 2004, MNRAS, 350, 1485
Magorrian J. et al., 1998, AJ, 115, 2285
Marconi A., Risaliti G., Gilli R., Hunt L. K., Maiolino R., Salvati M., 2004, MNRAS, 351, 169
Marinoni C., Hudson M. J., 2002, ApJ, 569, 101
Martini P., Weinberg D. H., 2001, ApJ, 547, 12
Matarrese S., Coles P., Lucchin F., Moscardini L., 1997, MNRAS, 286, 115
Menci N., Cavaliere A., Fontana A., Giallongo E., Poli F., Vittorini V., 2003, ApJ, 587, 63
Mo H. J., Fang L. Z., 1993, ApJ, 410, 493
Mo H. J., White S. D. M., 1996, MNRAS, 282, 347

Mo H. J., Mao S., White S. D. M., 1998, MNRAS, 295, 319
Monaco P., Salucci P., Danese L., 2000, MNRAS, 311, 279
Moscardini L., Matarrese S., Lucchin F., Rosati P., 2000, MNRAS, 316, 283
Moustakas L., Somerville R. S., 2002, ApJ, 577, 1
Navarro J. F., Frenk C. S., White S. D. M., 1997, ApJ, 490, 493 (NFW)
Norberg P. et al., 2002, MNRAS, 336, 907
Omont A., Cox P., Bertoldi F., McMahon R. G., Carilli C., Isaak K. G., 2001, A&A, 374, 371
Outram P. J., Hoyle F., Shanks T., Croom S. M., Boyle B. J., Miller L., Smith R. J., Myers A. D., 2003, MNRAS, 342, 483
Outram P. J., Shanks T., Boyle B. J., Croom S. M., Hoyle F., Loaring N. S., Miller L., Smith R. J., 2004, MNRAS, 348, 745
Peacock J. A., Dodds S. J., 1996, MNRAS, 267, 1020
Peacock J. A., Smith R. E., 2000, MNRAS, 318, 1144
Percival W. J., Miller L., McLure R. J., Dunlop J. S., 2001, MNRAS, 322, 843
Percival W. J., Scott D., Peacock J. A., Dunlop J. S., 2003, MNRAS, 338, L31
Porciani C., Giavalisco M., 2002, ApJ, 565, 24
Porciani C., Matarrese S., Lucchin F., Catelan P., 1998, MNRAS, 298, 1097
Richstone D. et al., 1998, Nat, 395, A14
Roche N. D., Dunlop J., Almaini O., 2003, MNRAS, 346, 803
Salpeter E. E., 1964, ApJ, 140, 796
Salucci P., Szuszkiewicz E., Monaco P., Danese L., 1999, MNRAS, 307, 637
Schirber M., Miralda-Escudè J., McDonald P., 2004, ApJ, 610, 105
Schneider D. P. et al., 2003, AJ, 126, 2579
Scoccimarro R., Sheth R. K., Hui L., Jain B., 2001, ApJ, 546, 20
Seljak U., 2000, MNRAS, 318, 203
Seljak U., 2002, MNRAS, 334, 797
Shanks T., Boyle B. J., 1994, MNRAS, 271, 753
Shanks T., Fong R., Boyle B. J., Peterson B. A., 1987, MNRAS, 227, 739
Shaver P. A., 1984, A&A, 136, L9
Sheth R. K., Diaferio A., 2001, MNRAS, 322, 901
Sheth R. K., Jain B., 2003, MNRAS, 345, 529
Sheth R. K., Tormen G., 1999, MNRAS, 308, 119
Silk J., Rees M. J., 1998, A&A, 331, L1
Tegmark M. et al., 2004, Phys. Rev. D, 69, 103501
Tremaine S. et al., 2002, ApJ, 574, 740
Vale A., Ostriker J. P., 2004, MNRAS, 353, 189
van den Bosch F. C., Mo H. J., Yang X., 2003, MNRAS, 345, 923
Yamamoto K., Suto Y., 1999, ApJ, 517, 1
Yang X., Mo H. J., van den Bosch F. C., 2003, MNRAS, 339, 1057
Yu Q., Tremaine S., 2002, MNRAS, 335, 965
Wyithe J. S. B., Loeb A., 2003, ApJ, 595, 614
Wyithe J. S. B., Loeb A., 2004, ApJ, submitted (astro-ph/0403714)
Zehavi I. et al., 2004, ApJ, 608, 16
Zel'dovich Ya. B., Novikov I. D., 1964, Sov. Phys. Dokl., 158, 811
Zheng Z., 2004, ApJ, 610, 61

APPENDIX A: MASS DISTRIBUTION OF QUASAR HOST HALOES

In this section, we use a few observational results to derive the conditional probability distribution of the host halo mass, M, for a quasar with given absolute magnitude M_{b_J}.

A1 From photographic to Johnson *B* magnitudes

We start from converting b_J fluxes into standard B magnitudes. In general, $B \simeq b_\mathrm{J} + 0.3(B\text{–}V)$ (Blair & Gilmore 1982; Colless et al. 2001), and the rest-frame colour index for quasars is $B\text{–}V \simeq 0.22$ (Cristiani & Vio 1990). In what follows, we then assume

$$M_\mathrm{B} = M_{b_\mathrm{J}} + 0.07, \qquad \text{(A1)}$$

which is in good agreement with Brotherton et al. (2001). Note that the amplitude of the correction is comparable with the statistical error which affects the magnitude determination in the 2dFGRS (Colless et al. 2001; Norberg et al. 2002) which uses the same UKST photographic plates as the 2QZ. It is then reasonable to expect that also quasar photometry in the 2QZ is affected by typical errors of ~ 0.1 mag (e.g. Corbett et al. 2003).

A2 Bolometric corrections

In order to use equation (20) to infer the mass of the black holes which power 2QZ quasars, we need to convert their absolute B magnitudes into bolometric luminosities. Bolometric corrections for a sample of X-ray selected quasars lying at $z < 1$ have been derived in a seminal paper by Elvis et al. (1994). Because observations show that quasar spectra do not evolve with z (e.g. Bechtold et al. 1994), it is common practice to apply these corrections also to high-redshift quasars. It has been recently pointed out, however, that the bolometric corrections by Elvis et al. (1994) are seriously affected by systematics and should be revised downwards (e.g. Fabian & Iwasawa 1999; Elvis, Risaliti & Zamorani 2002). For this reason we use here the results by McLure & Dunlop (2004) who, adopting the revised template spectrum by Elvis et al. (2002), estimated the bolometric corrections for 1136 quasars at $0.5 < z < 0.8$ extracted from the SDSS. Corrections from the B band have then been computed using a subsample of 372 objects common to the 2dF and SDSS surveys. When combined with equation (A1), their best-fitting relation gives

$$\log_{10}\left(\frac{L_\mathrm{bol}}{10^{46}\,\mathrm{erg\,s^{-1}}}\right) = 0.21 - 0.38\,(M_{b_\mathrm{J}} + 25) \qquad \text{(A2)}$$

and the corresponding rms variation at fixed M_{b_J} is 0.14. Within the quoted uncertainties, this is perfectly consistent with the recent results by Marconi et al. (2004).[14]

A3 Eddington ratio and distribution of black hole masses

Observational estimates of the Eddington ratio, η, require: (i) using some dynamical tracer to determine the black hole mass (and thus the Eddington luminosity); (ii) measuring the quasar luminosity in a given band, L_i; (iii) applying the corresponding bolometric correction, β_i^bol; (iv) calculating $\eta \propto \beta_i^\mathrm{bol}\; L_i/M_\mathrm{bh}$. Given this complexity, measurements of η are rather uncertain and sensitive to a number of sources of systematic errors. Recent determinations, however, tend to lie in the same ballpark and suggest that η mildly increases with z (Dunlop et al. 2003; McLure & Dunlop 2004). For consistency with Appendix A2, we use here the results by McLure & Dunlop (2004) who combined virial estimates of black hole masses with new bolometric corrections to infer the Eddington ratio for a large sample of quasars from the SDSS. From their results we infer that, for $0.8 < z < 2.1$, the probability density function for $\log_{10}\eta$ is well approximated by a Gaussian distribution with mean $0.21\,z - 0.80$ and variance ~ 0.3. This corresponds to $\langle\eta\rangle = 10^{0.21z-0.65}$. These results are also supported by other indirect determinations of η. By requiring the mass function of relic black holes (as inferred from the X-ray background) to match its local counterpart, Marconi et al. (2004) found that $0.1 \lesssim \eta \lesssim 1.7$ (with a preferred value of $\eta \sim 0.5$). Once the different bolometric corrections are accounted for, these values are in extremely good agreement with the results from

[14] The bolometric corrections by Marconi et al. (2004) are roughly two-thirds of those by Elvis et al. (1994) and correspond to $\log_{10}(L_\mathrm{bol}/10^{46}\,\mathrm{erg\,s^{-1}}) = 0.37 - 0.40\,(M_{b_\mathrm{J}} + 25)$ with a scatter at fixed M_{b_J} of 0.3.

McLure & Dunlop (2004). Similarly, Yu & Tremaine (2002) have shown that the local mass density in black holes is consistent with the integrated luminosity density of quasars if they accrete mass nearly at the Eddington rate at redshifts $z \gtrsim 2$.

A4 Distribution of black hole masses

The conditional probability distribution of $\log_{10} M_{\rm bh}/{\rm M}_{\odot}$ for a given $L_{\rm bol}$ is thus obtained by combining equation (20) with the observationally determined distribution of η

$$P\left(\log_{10}\frac{M_{\rm bh}}{{\rm M}_{\odot}}|L_{\rm bol}\right) = 0.73 \times \exp\left\{-\frac{[\log_{10}(M_{\rm bh}/{\rm M}_{\odot}) - f]^2}{0.6}\right\} \quad \text{(A3)}$$

with $f = 8.70 - 0.21\,z + \log_{10}(L_{\rm bol}/10^{46}\ {\rm erg}\ \ {\rm s}^{-1})$. For consistency, in order to estimate the black hole mass associated with a quasar of given absolute magnitude $M_{b_{\rm J}}$, we combine equations (A2) (including its associated scatter) and (A3), which have been derived from the same data set. This implies that a quasar with $M_{b_{\rm J}} = -25$ corresponds to a mean black hole mass of $5.13 \times 10^8\ {\rm M}_{\odot}$ at $z = 1$ and of $3.16 \times 10^8\ {\rm M}_{\odot}$ at $z = 2$. Note that for the typical redshift and magnitude ranges spun by our sample, $6 \times 10^7\,{\rm M}_{\odot} \lesssim \langle M_{\rm bh}|M_{b_{\rm J}}\rangle \lesssim 3 \times 10^9\,{\rm M}_{\odot}$. This interval is consistent with the masses inferred from dynamical measures in the local Universe (e.g. Tremaine et al. 2002 and references therein) and from the analysis of emission linewidths in the 2QZ (Corbett et al. 2003).

A5 Mass of host haloes

Taking a step further, we can estimate the probability distribution that a quasar of a given luminosity is hosted by a dark matter halo of mass M. Following Ferrarese (2002), and see also Baes et al. (2003), this is obtained by assuming that a statistically significant correlation links $M_{\rm bh}$ and M.

Black hole masses are found to be tightly correlated with the velocity dispersion of their host spheroid, $\sigma_{\rm sph}$ (Ferrarese & Merritt 2000; Gebhardt et al. 2000). The most recent determination considers ~ 30 galaxies with secure detections of supermassive black holes (Tremaine et al. 2002). Observations also provide evidence for a correlation between $\sigma_{\rm sph}$ and the circular velocity in the flat part of the rotation curve of the host galaxy (Ferrarese 2002; Baes et al. 2003). By combining the $M_{\rm bh}$–$\sigma_{\rm sph}$ and $\sigma_{\rm sph}$–$v_{\rm c}$ relations, Baes et al. (2003) find

$$\frac{M_{\rm bh}}{{\rm M}_{\odot}} = 10^{7.24\pm0.17}\left(\frac{v_{\rm c}}{200\,{\rm km\,s^{-1}}}\right)^{4.21\pm0.60}. \quad \text{(A4)}$$

This purely observational relation can be used to link $M_{\rm bh}$ with the mass of the host halo. In order to do this, however, we need to express $v_{\rm c}$ in terms of M, which is a formidable task. As a first-order approximation, we can assume an equilibrium configuration for the dark matter density profile in haloes. Both the singular isothermal sphere and models derived from numerical simulations (e.g. NFW) provide good starting points. However, detailed modelling of the rotation curve requires accounting for the distribution and physics of baryons (e.g. Mo, Mao & White 1998). In fact, the gas contribution can be dominant in the innermost regions of galaxies. Moreover, the condensation towards the centre of the dissipative material redistributes, through gravity, the collisionless matter.

For simplicity, we consider equilibrium profiles which only contain dark matter and we account for the presence of baryons in an approximate way. The circular velocity at the virial radius of each halo is

$$\frac{v_{\rm vir}}{159.4\,{\rm km\,s^{-1}}} = \left(\frac{M}{10^{12}\,h^{-1}\,{\rm M}_{\odot}}\right)^{1/3}\left(\frac{E_z^2\,\Delta_z}{18\,\pi^2}\right)^{1/6}, \quad \text{(A5)}$$

where $E_z^2 = \Omega_0(1+z)^3 + \Omega_\Lambda$, and Δ_z is the ratio between the mean density of the halo and the critical density of the Universe (both evaluated at redshift z). For a spherical collapse, this function can be approximated as $\Delta \simeq 18\pi^2 + 82x - 39x^2$ with $x = \Omega_{\rm m}(z) - 1$ and $\Omega_{\rm m}(z) = \Omega_0(1+z)^3/E_z^2$ (Bryan & Norman 1998).

A truncated singular isothermal sphere has a constant circular velocity profile $v_{\rm c} = v_{\rm vir}$, while for an NFW density profile

$$\frac{v_{\rm c}(\mathcal{R})}{v_{\rm vir}} = \left[\frac{1}{\mathcal{R}}\frac{F(\mathcal{C}\mathcal{R})}{F(\mathcal{C})}\right]^{1/2}, \quad \text{(A6)}$$

where $\mathcal{R} = r/r_{\rm vir}$, $F(x) = \ln(1+x) - x/(1+x)$ and $\mathcal{C}$ is the concentration parameter of the halo. In this case, the circular velocity vanishes when $\mathcal{R} \to 0$, reaches a maximum at $\mathcal{R} \simeq 2.16/\mathcal{C}$ and matches the virial velocity at $\mathcal{R} = 1$. Two questions naturally arise. (i) What is the value of $\mathcal{R}$ which corresponds to the observed circular velocities? (ii) What is the contribution of the baryons at this radius? These are the main uncertainties of our analysis.

For galaxies with H I rotation curves, $v_{\rm c}$ is typically measured at a few tens of kpc from the centre, well beyond the optical radius (a few kpc). On the other hand, the present-day virial radius of a halo with $M = 10^{13}\ {\rm M}_{\odot}$ is $r_{\rm vir} = 0.56$ Mpc. In other words, the largest scales sampled by rotation-curve measurements are nearly a factor of 10 smaller than the virial radius. Using galaxy–galaxy lensing data from the SDSS, Seljak (2002) has shown that, for galaxies above L_*, $v_{\rm c}$ decreases significantly from the optical radius of a galaxy to the virial radius of its host halo. This result is independent of the morphological type and probably suggests that baryons contribute significantly to the circular velocity at the optical radius and that density profiles for the dark matter are highly concentrated (as expected in CDM models at $z = 0$). Seljak (2002) also found a clear trend for the ratio $\psi = v_{\rm c}/v_{\rm vir}$ with halo mass. Typical values are $\psi \sim 1.8$ for $M \sim 3 \times 10^{11}\ {\rm M}_{\odot}$, $\psi \simeq 1.4 \pm 0.2$ for $M \sim 10^{13}\ {\rm M}_{\odot}$ and $\psi < 1$ for cluster masses. This is in good agreement with the predictions of CDM models, because the dark matter concentration is expected to decrease with the halo mass and the baryonic contribution is expected to become less and less important.

Assuming that the observed $v_{\rm c}$ corresponds to the maximum value of the rotational velocity profile in an NFW halo tends to underestimate Seljak's results. Using equations (9) and (13) in Bullock et al. (2001), we find that, at $z = 0$, this assumption corresponds to $\psi = 1.3\,(\mathcal{C} \sim 14)$ for $M \sim 3 \times 10^{11}\ {\rm M}_{\odot}$ and $\psi = 1.2\,(\mathcal{C} \sim 9)$ for $M \sim 10^{13}\ {\rm M}_{\odot}$. Anyway, these results show the correct trend with the halo mass: smaller, more concentrated haloes are associated with larger values for ψ. It is worth noticing, however, that the candidate hosts of our quasars (haloes with $M \sim 10^{13}\ {\rm M}_{\odot}$ at $0.8 < z < 2.1$) are expected to be much less concentrated ($\mathcal{C} \sim 3$–5) than their present-day counterparts. In this case, the maximum value of the rotational velocity is only 2–15 per cent higher than $v_{\rm vir}$. This motivates the choice $\psi \simeq 1$ as a viable alternative to the low-redshift results by Seljak (2002).

We have now collected all the elements necessary to estimate the conditional probability distribution of the host halo mass, M, for a quasar with given absolute magnitude $M_{b_{\rm J}}$: $\mathcal{P}(M|M_{b_{\rm J}})$. In brief, (i) we assume that equations (A2), (A3) and (A4), which have been determined at lower redshifts, are still valid for the host galaxies of our 2QZ quasars at $0.8 < z < 2.1$. Their combination (including the scatter in each of them) is used to determine the probability distribution of v_c. (ii) We then convert circular velocities into halo masses by selecting a value of ψ and using equation (A5). To match the results by Seljak (2002), we assume a Gaussian distribution for ψ with mean value of 1.4 and scatter of 0.2 (case A). Alternatively, based on the estimated low concentration of high-redshift haloes, we assume that $\psi = 1$ (case B).

APPENDIX B: HALO OCCUPATION DISTRIBUTION FROM SEMI-ANALYTICAL MODELS OF GALAXY FORMATION

We use here semi-analytical models of galaxy formation to gain an insight into the problem of choosing a functional form for the first two moments of the quasar halo occupation distribution.

B1 Halo occupation number

There is evidence that, at high redshift, quasars are associated with star-forming galaxies (e.g. Omont et al. 2001; Hutchings et al. 2002). It is then plausible to expect that the halo occupation properties of quasars might share some similarities with those of galaxies which show active star formation in their nuclear region. As an example, we derive here the function $N(M)$ from the semi-analytical models of the GalICS I collaboration (Hatton et al. 2003) at $z = 1.08$ (roughly corresponding to the median value for our low-redshift sample). Results for galaxies with a bulge star formation rate, $\psi_{\rm bulge}$, which is larger than $10\,{\rm M}_\odot\,{\rm yr}^{-1}$ are shown in Fig. B1. The choice of such a threshold for $\psi_{\rm bulge}$ is motivated by the fact that the mean density of these objects ($\sim 12 \times 10^{-6}\,h^3\,{\rm Mpc}^{-3}$) is comparable with the mean density of our low-redshift quasar sample. In order to improve the statistics, in Fig. B1 we also show the function $N(M)$ for galaxies

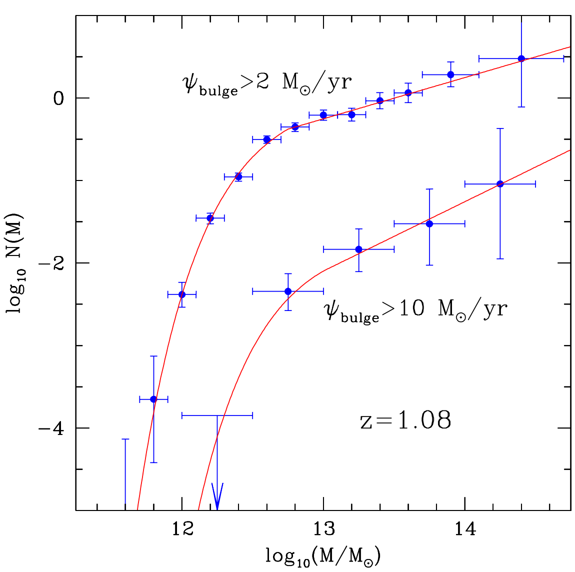

Figure B1. The halo occupation number of galaxies which at $z = 1.08$ are actively forming stars in the bulge as obtained from semi-analytical models of the GalICS collaboration. Data points correspond to the estimated $N(M)$, vertical error bars mark the associated 1σ uncertainties (assuming Poisson statistics for both the number of galaxies and the number of haloes in a bin), while the horizontal error bars denote the size of the mass bins. Arrows mark the upper limit for $N(M)$ in the bins where we measure $N = 0$. The solid lines show a fit to the data obtained by using the function in equation (B1). For $\psi_{\rm bulge} > 10\,{\rm M}_\odot\,{\rm yr}^{-1}$, the best-fitting parameters are $\alpha = 0.85$, $M_0 = 10^{13}\,{\rm M}_\odot$ and $N_0 = 8 \times 10^{-3}$. On the other hand, for $\psi_{\rm bulge} > 2\,{\rm M}_\odot\,{\rm yr}^{-1}$, we obtain $\alpha = 0.5$, $M_0 = 10^{12.75}\,{\rm M}_\odot$ and $N_0 = 0.42$.

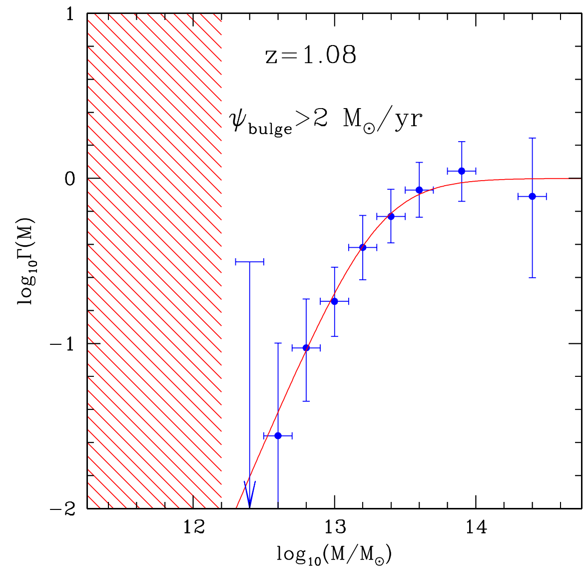

Figure B2. As in Fig. B1 but for the function $\Gamma(M)$. The fitting function represented with a solid line is given in equation (B2) and corresponds to the best-fitting parameters $\gamma_s = 2$ and $M_s = 10^{13.3}\,{\rm M}_\odot$. The shaded region indicates the mass range where the function Γ is totally undetermined.

with $\psi_{\rm bulge} > 2\,{\rm M}_\odot\,{\rm yr}^{-1}$. In both cases, the halo occupation number is well approximated by a power law with a cut-off at small virial masses. For instance, the function

$$N(M) = N_0 \times \begin{cases} (M/M_0)^\alpha & \text{if } M \geqslant M_0 \\ \exp\,[1 - (M_0/M)] & \text{if } M < M_0 \end{cases} \quad \text{(B1)}$$

very closely matches the results of the semi-analytical models in Fig. B1. This is in good agreement with equation (18) where a sharp cut-off replaces the exponential decline at small masses.

B2 Scatter of $P_N(M)$

In this section, we use the previously introduced samples of star-forming galaxies to study the second moment of the halo occupation distribution. We first note that there is not a single halo in the GalICS I sample which contains more than one galaxy with $\psi_{\rm bulge} > 10\,{\rm M}_\odot\,{\rm yr}^{-1}$ at $z = 1.08$. In other words, the data (within extremely large error bars) are consistent with $\Sigma^2 = 0$. This is clearly an effect of the small number statistics. On the other hand, the results for $\psi_{\rm bulge} > 2\,{\rm M}_\odot\,{\rm yr}^{-1}$ are much more significant. In this case, the numerical results are well approximated by the function

$$\Gamma(M) = \left(\frac{M}{M_s}\right)^{\gamma_s} \left[1 + \left(\frac{M}{M_s}\right)^{\gamma_s}\right]^{-1}, \quad \text{(B2)}$$

which scales as a power law for $M \ll M_s$ and approaches 1 for $M \gg M_s$ (see Fig. B2). In agreement with studies of low-redshift galaxies (e.g. Sheth & Diaferio 2001; Berlind & Weinberg 2002; Berlind et al. 2003), the scatter of $P_N(M)$ is then strongly subPoissonian for haloes which, on average, contain less than one object, and nearly Poissonian for larger haloes. We find that, adopting $N(M_s) = 0.75$ as an operative definition for M_s, equation (B2) with $\gamma_s = 2$ accurately describes the second moment of the halo occupation distribution for rare galaxies at $z \simeq 1$. This result does not depend on the details of the galaxy population considered (star formation rate, colour, etc.).

This paper has been typeset from a TEX/LATEX file prepared by the author.